

# Highly transparent silanized cellulose aerogels for boosting energy efficiency of glazing in buildings

Received: 14 August 2022

Accepted: 7 February 2023

Published online: 16 March 2023

 Check for updates

Eldho Abraham<sup>1</sup>, Vladyslav Cherpak<sup>1</sup>, Bohdan Senyuk<sup>1,2</sup>, Jan Bart ten Hove<sup>1</sup>, Taewoo Lee<sup>1</sup>, Qingkun Liu<sup>1</sup> & Ivan I. Smalyukh<sup>1,2,3,4</sup> 

To maintain comfortable indoor conditions, buildings consume ~40% of the energy generated globally. In terms of passively isolating building interiors from cold or hot outdoors, windows and skylights are the least-efficient parts of the building envelope because achieving simultaneously high transparency and thermal insulation of glazing remains a challenge. Here we describe highly transparent aerogels fabricated from cellulose, an Earth-abundant biopolymer, by utilizing approaches such as colloidal self assembly and procedures compatible with roll-to-roll processing. The aerogels have visible-range light transmission of 97–99% (better than glass), haze of ~1% and thermal conductivity lower than that of still air. These lightweight materials can be used as panes inside multi-pane insulating glass units and to retrofit existing windows. We demonstrate how aerogels boost energy efficiency and may enable advanced technical solutions for insulating glass units, skylights, daylighting and facade glazing, potentially increasing the role of glazing in building envelopes.

To provide desired indoor conditions irrespective of the outdoor environment at little or no additional energy supply, building envelopes need to minimize the interior–exterior exchange of energy through thermal conduction, convection and emission<sup>1–4</sup>. To achieve this with glazing is especially challenging because of the typical stringent requirements on visible-range transparency and haze<sup>5,6</sup>. While current approaches to this challenge utilize the insulating glass units (IGUs) with air or fill gas<sup>5–8</sup>, high thermal-barrier performance of such IGUs requires large gap thickness between glass panes, which in turn is limited by gas convection, number of panes and structural constraints. The use of much thinner vacuum-insulated glass units, on the other hand, is limited by the seal integrity and high costs<sup>9,10</sup>. Low-emissivity silver and other coatings allow for limiting the energy loss due to black-body-like electromagnetic emissivity originating from the room-temperature building's interior<sup>5–10</sup>, though they can capture only a fraction of escaping energy at a cost of deteriorating

visible-range transparency. Aerogels, highly thermally insulating materials used in applications ranging from pipe insulation to a Mars rover<sup>11–13</sup>, have been highly sought after for applications inside IGUs as a solid material replacement for gas fillers<sup>14–19</sup> because they stand out as a class of materials capable of outperforming still air and other gas fillers as efficient thermal barriers<sup>20–24</sup>. However, aerogels are typically mechanically fragile and strongly scatter light<sup>12,13,25–29</sup>. Manufacturing aerogels with low haze, high transparency and mechanical robustness at building-relevant scales and costs also remained a challenge<sup>30</sup>. Development of transparent aerogels, including cellulose-based ones<sup>25,28–31</sup>, remained limited to small scales while also featuring haze and transparency characteristics still inadequate for uses in most types of glazing. While the technological solutions for controlling thermal-range emissivity are highly adequate and widely used<sup>5–9</sup>, and the recent advent of the electrochromic approaches promise to address the needs of solar gain and privacy control<sup>32–34</sup>, the lack of good

<sup>1</sup>Department of Physics, University of Colorado, Boulder, CO, USA. <sup>2</sup>International Institute for Sustainability with Knotted Chiral Meta Matter, Hiroshima University, Higashihiroshima, Japan. <sup>3</sup>Materials Science and Engineering Program, University of Colorado, Boulder, CO, USA. <sup>4</sup>Renewable and Sustainable Energy Institute, National Renewable Energy Laboratory and University of Colorado, Boulder, CO, USA. ✉e-mail: [ivan.smalyukh@colorado.edu](mailto:ivan.smalyukh@colorado.edu)

transparent thermal barriers strongly limits the energy efficiency of window technologies<sup>5–9</sup>.

Here we demonstrate scalable manufacturing of highly transparent silanized cellulose aerogels (SiCellAs) with material characteristics adequate for glazing applications. These highly thermally insulating SiCellA materials, sandwiched between glass panes, may allow for windows with high resistance  $R$  to heat flow, such as  $R_b = 5 \text{ h ft}^2 \text{ }^\circ\text{F Btu}^{-1}$  (Imperial units common for North America, where Btu stands for a British thermal unit) and  $R_s \approx 0.9 \text{ m}^2 \text{ K W}^{-1}$  (SI units). SiCellA may help to achieve such high- $R$  insulation for a geometric form factor of a conventional double-pane IGU and may enable glazing for daylighting and skylights, potentially exceeding the current standards and targets not only for windows but even for building walls<sup>1–4,7</sup>. While the deployment of IGUs with air or other gas fillers is limited by convection at large inter-pane gaps and by reflections of light from glass–air interfaces of multi-pane IGUs, no such intrinsic limitations exist for SiCellA-based IGUs. This glazing may allow for the building envelopes to be designed to better take advantage of external conditions to provide natural occupant comfort. We show how SiCellA films can be used as IGU fillers and in multi-pane IGU designs to replace the inner glass panes and are fully compatible with the existing solutions for thermal-range emissivity and solar gain control. We envisage that SiCellAs will provide a holistic solution to the energy-management challenges that building technologies face, potentially even helping the next generation of buildings harness energy from the environment by allowing for better taking advantage of solar heating and natural lighting through the increased use of glazing<sup>30</sup>, provided that economically viable manufacturing of SiCellA can be achieved.

## Fabrication of window-scale nanostructured SiCellA materials

Our transparent, thermally super-insulating SiCellA materials are envisaged to boost the efficiency of pre-existing windows and enable advanced window products (Fig. 1a,b), as we demonstrate using prototypes of SiCellA-based retrofit films and IGUs at window-relevant scales (Fig. 1c–e and Supplementary Figs. 1 and 2). The SiCellA films readily adhere to the surfaces of plastic films and glass panes due to electrostatic charging. A thin film of SiCellA (Fig. 1c) allows for boosting the thermal barrier performance of a single-pane window when used as a retrofit laminated on its inner surface as vividly revealed by thermal imaging of the exterior glass surface temperature during winter (Fig. 1f). The temperature of the outer surface of retrofitted panes is measured to be lower than that of similar panes without retrofits because of more effective blocking of the heat transfer through the window enabled by the installation of a SiCellA retrofit (Fig. 1f). Hot and cold boxes (Methods) which mimic the interior–exterior heat exchange during summers and winters, respectively, illustrate similar superior thermal barrier performance enabled by SiCellAs when laminated atop a single-pane glass or inserted into the gap of a double-pane IGU (Fig. 1g,h).

To fabricate SiCellA materials, wood-pulp-derived cellulose nanofibres are processed by 2,2,6,6-tetramethylpiperidine-1-oxyl radical (TEMPO)-mediated oxidation of native cellulose<sup>25,35–37</sup> (Methods and Supplementary Fig. 3). Consequently, the surface charges associated with the carboxylate anion preclude aggregation<sup>25,30</sup> of the nanofibres and allow formation of stable aqueous colloidal dispersions at varying concentrations, which can be poured into moulds of desired shapes and sizes (Methods and Supplementary Figs. 3 and 4). Adding acid interlinks these nanofibres by hydrogen bonds between the carboxyl groups, transforming the colloidal dispersion into a hydrogel (Supplementary Fig. 4b) with a network of sparse nanofibres<sup>25</sup>. Next, we exchange the fluid medium within the gel by replacing water with isopropanol or ethanol (Fig. 2a,b and Supplementary Fig. 4c,d), and the gel is then supercritically dried to form an aerogel (Fig. 2c and Supplementary Fig. 5a–d)<sup>30</sup>. These fabrication procedures are highly scalable (Fig. 2a–c) and compatible with roll-to-roll processing, combining simple steps such as moulding to define the volume of the desired

hydrogel, solvent exchanges at modestly elevated temperatures (Methods and Supplementary Fig. 4), rolling and drying the gels atop plastic support in rolls (Supplementary Fig. 5b,d,f). Moreover, they allow for preventing aggregation of cellulose nanofibres during gelation or drying so that initially transparent colloidal dispersions remain transparent in hydrogel and aerogel states (Fig. 2d,e and Supplementary Fig. 5).

An important part of a fabrication procedure is that cellulose surfaces are silanized, which can be done by vapour-phase functionalization (Fig. 2f) after the supercritical drying or at the hydrogel stage, before drying, with details of both approaches described in Methods, Fig. 2f and Supplementary Fig. 4e–k. Silanization procedures make SiCellAs superhydrophobic (Supplementary Video 1; note the contact angle of the water droplet  $>150^\circ$  revealed in Fig. 2h), a highly desirable property for window applications, as also revealed by infrared spectroscopy through analysing the presence or strength of corresponding absorption lines (Fig. 2g).

Nanoscale characterization provides insights into the formation and structure of SiCellA materials (Fig. 3). The individualized cellulose nanofibres are well-defined rod-like particles with 4–6 nm width and hundreds to thousands nanometres length (Fig. 3a). The fabrication procedures of gelation, surface modification, solvent exchanges and drying transform the initial colloidal dispersions of such nanorods into gels with nanoscale morphology featuring networks of thin fibres, with inter-fibre pores typically smaller than 100 nm (Fig. 3b–d and Supplementary Video 2). By controlling the initial concentration of cellulose nanofibres, we can vary the porosity of SiCellA (Fig. 3e), which is linearly related to the mass density of the material. Nitrogen adsorption–desorption analysis is consistent with the direct nanoscale imaging, yielding quantitative information about SiCellA's porous morphology (Fig. 3f,g, Supplementary Fig. 6 and Supplementary Video 2) associated with a network of interlinked nanofibres (Fig. 3h).

## Optical, thermal and mechanical properties of SiCellA

Modern windows and skylights are expected to effectively separate the controlled indoor environment from the building's exterior, while serving their primary functions enabled by transparency, setting requirements for respective material properties<sup>1–9</sup>. To probe these properties, we show that a free-standing slab of SiCellA features very high visible-range transmissivity, within 97–99%, much higher than ~92% of a single clear glass (Fig. 4a–c, Supplementary Fig. 1 and Supplementary Table 1). Additionally, the haze coefficient is low, typically within 1–3%, depending on the thickness of the SiCellA slab (Fig. 4a,b). Highly transparent, low-scattering slabs of varying thickness can be made (Fig. 4b and Supplementary Videos 3 and 4). This optical transparency stems from the nanoscale structure of SiCellA (Fig. 3 and Supplementary Video 2), where all length scales of aerogel morphology are much smaller than the wavelength of light in the visible spectral range.

The very high porosity of SiCellA, with the content of the solid being only ~1% and that of air ~99%, makes effective refractive indices of SiCellA materials and air close (Fig. 4d). Because of this low refractive index ~1.0025 (compare that of air ~1.0003 and glass ~1.52), the SiCellA–air interfaces reflect much less light than glass–air interfaces so that SiCellA's light transmission is high throughout the visible and near-infrared spectral ranges (Fig. 4a,b,e). Because of the refractive index-matching properties of SiCellA and air, prisms of these materials exhibit very small deflection angles while light follows Snell's law at the aerogel–air interfaces (Fig. 4f and Supplementary Video 3). The colour rendering index, which quantifies the impact of a material or a window on the perception of natural colours<sup>38,39</sup> is very high, ~99%, so that the natural colours are preserved. Furthermore, SiCellA materials can be cut to desired shapes using a regular razor while retaining high transparency (Fig. 4c,f) and can be moulded to adopt a large variety of geometric shapes and dimensions from millimetres to metres while preserving low haze and high transparency (Figs. 1 and 4c,g–j).

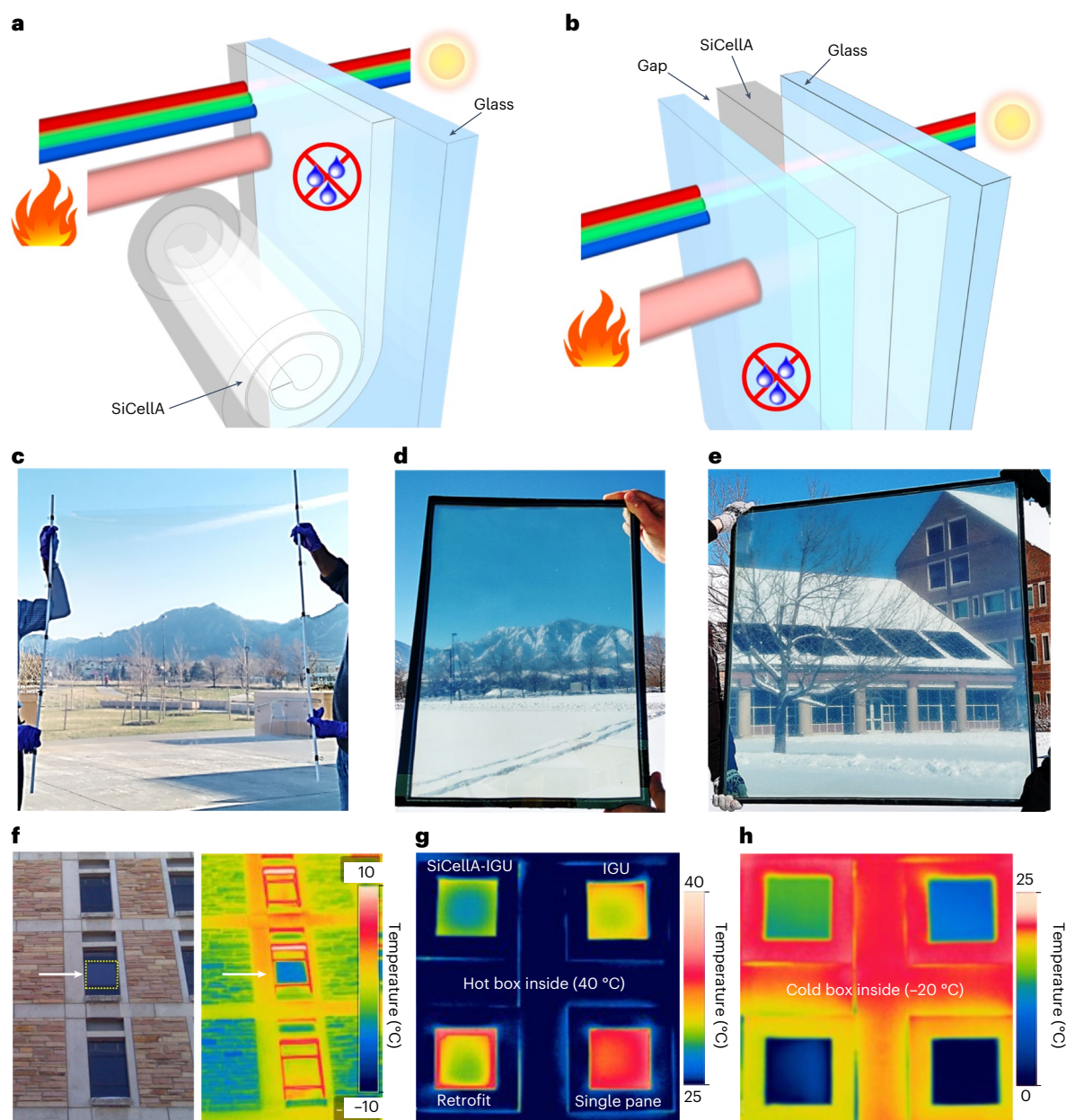


**Fig. 1 | SiCellA-based window retrofits and IGUs.** **a, b**, Schematic drawings of a window retrofitted with a SiCellA film (**a**) and an IGU with a SiCellA film inserted between glass panes (**b**). Schematics depict how window products can be used to boost thermal insulation and condensation resistance while maintaining visible-range transparency. **c**, Square-metre, 1.5 mm-thick SiCellA with 99.2% porosity adhered to an optically clear plastic film. **d, e**, Photos of 36 cm × 51 cm (**d**) and square-metre (**e**) double-pane IGUs with LoE-366 coatings on one glass pane and 3 mm-thick SiCellA films attached to a surface of the other glass panes. Note that the slight colouring in **d** and **e** comes from the LoE-366 coated glass used in these IGUs. **f**, Single-pane window retrofitted with a 72.1 cm × 71.4 cm

SiCellA 1.5 mm-thick film (indicated by a white arrow and outlined by a dashed line) and photographed from outside with both a regular photo camera (left) and a thermal imaging camera (right) in a building on the University of Colorado campus. Temperature is coded according to a colour scale. **g, h**, Infrared thermal imaging photos of different types of fenestration mounted in the openings of 0.78 m × 0.68 m × 0.43 m hot (**g**) or cold (**h**) boxes with the inside temperature set at 40 °C (**g**) and -20 °C (**h**). 'SiCellA-IGU' marks a double-pane IGU with a SiCellA aerogel film; 'IGU' marks a double-pane IGU without SiCellA; 'Retrofit' marks a single 3 mm-thick glass pane retrofitted with a SiCellA film; 'Single pane' marks a single 3 mm-thick glass pane.

While minimally affecting the visible light transmission (Fig. 4), SiCellA can serve as an excellent thermal barrier (Fig. 5), capable of boosting the window's heat transfer resistance  $R$  and reducing the  $U$ -factor measuring how well a window insulates,  $U = 1/R$ . The aerogel's thermal conductivity and  $R$  depend on porosity<sup>30,40</sup> and vary with temperature (Fig. 5a,b). For appropriately selected porosities, SiCellA outperforms thermal barrier properties of still air, and its performance does not suffer from convection-related problems characteristic of air and other gas fillers<sup>40</sup>, as we discuss below in the contexts of window

products. A vivid demonstration of excellent thermal insulation is obtained by placing the slabs of aerogel of different thickness and shapes on top of hot surfaces (Fig. 5c).

The nanoscale morphology of SiCellA is such that air molecules collide more often with the cellulose network than with each other so that a gas thermal conduction is greatly reduced as compared with that of bulk air, whereas the poor thermal contacts between fibres of the cellulose network minimize the thermal conduction through the (~1% by volume) solid component<sup>30,40</sup>. In addition to these two

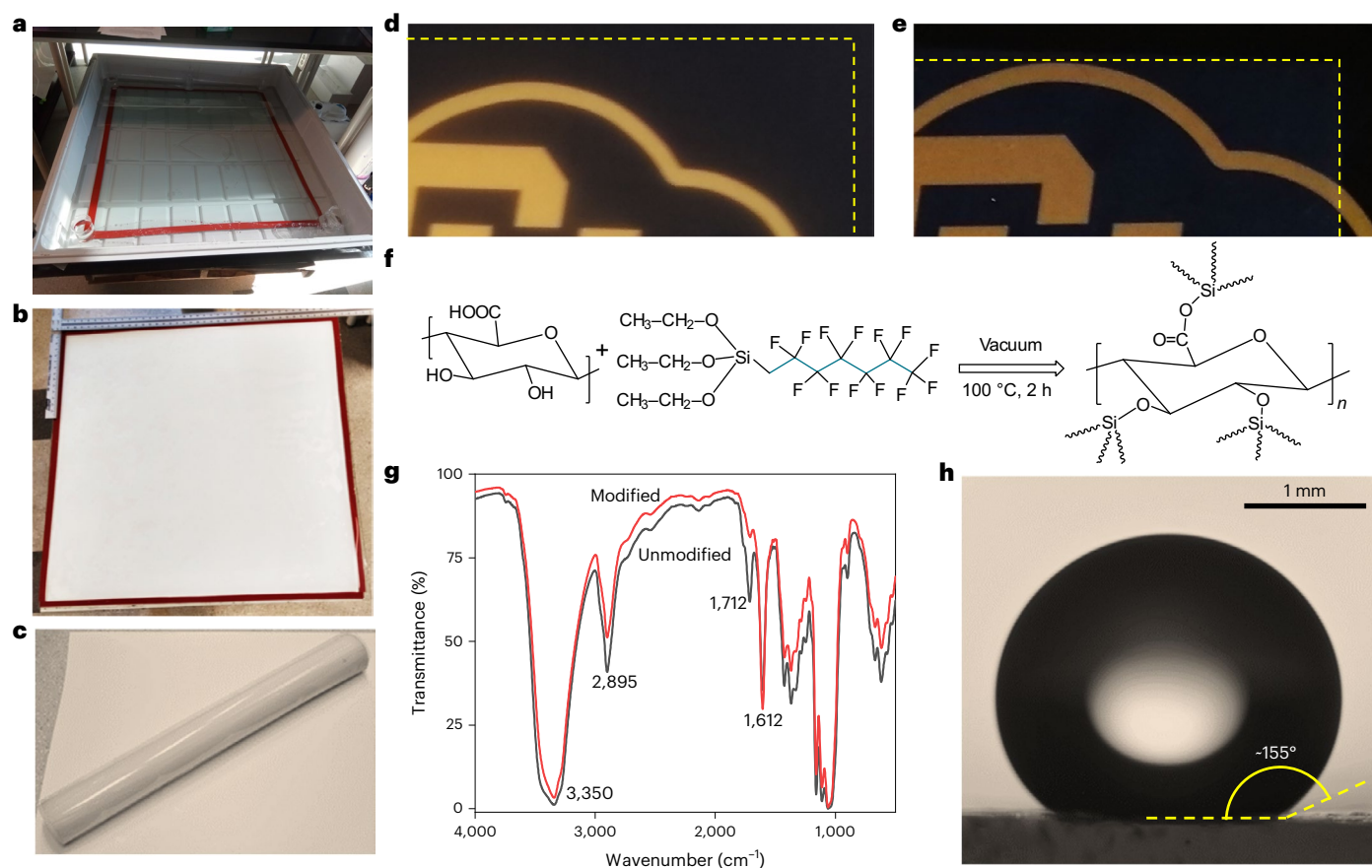


**Fig. 2 | Fabrication of superhydrophobic SiCellAs at window scales.** **a**, Gelation of a square-metre gel followed by solvent exchange in a 40 l bath. Red 3 mm-thick rubber spacers constitute borders of a flat mould. **b, c**, Square-metre hydrogel film atop a supporting white Mylar sheet photographed before rolling into a roll for drying in a critical-point dryer (**b**) and an ensuing tightly rolled 3 mm-thick SiCellA film on top of a Mylar sheet after drying (**c**). **d, e**, Three mm-thick hydrogel (outlined by a dashed line) shown in **b** floating in water (**d**) and the corresponding

3 mm-thick aerogel (outlined by a dashed line) after drying (**e**). **f**, Schematic of the vapour-phase silanization of the aerogel. **g**, Infrared transmission spectra of unmodified and modified aerogels, with a carboxylate at  $1,712 \text{ cm}^{-1}$  highly diminished in the aerogel after the surface modification. **h**, A photo of a water droplet on a SiCellA film's surface with a contact angle  $-155^\circ$  measured and marked on the image.

factors and measured low thermal conductivity, different from air, SiCellAs obstruct transmission of thermal-range radiation so that the radiative heat transfer is reduced, too (Fig. 5d,e). The aerogels based on pristine cellulose are somewhat transparent in parts of the thermal range, but silanization of their surfaces substantially reduces this transparency (Fig. 5d)<sup>30</sup>, thus further boosting the thermal barrier properties of SiCellA as compared with cellulose aerogels without silanization<sup>25</sup> as we quantify with the help of transmissive emittance weighted over the spectrum of thermal black-body radiation at room temperature (Fig. 5e).

In general, the solid networks and gas conduction are the two main contributions to the overall thermal conductivity of aerogels<sup>25,40</sup>, with the former decreasing and the latter increasing with porosity, so that typically a minimum in the thermal conductivity versus porosity is observed, though not within the range of porosities for which we could preclude aggregation of nanofibres and assure low haze. Additional research and development may allow for further reducing thermal conductivity by making SiCellA with other porosities, though here we focus on materials with non-aggregated nanofibres that also give very high optical transparency. We also note that silanization somewhat alters the thermal conductivity values as compared with aerogels made of pristine cellulose nanofibres<sup>25</sup>. Although many aerogels can exhibit rather low thermal conductivity<sup>25,29,41,42</sup>, SiCellA uniquely combines this property with very high visible transparency and low haze, as needed for window applications.

SiCellAs are optically anisotropic (birefringent, with the difference between extraordinary and ordinary refractive indices  $\sim 4 \times 10^{-3}$ ) because they are prepared through gelation of nematic colloidal dispersions of oxidized cellulose nanofibres (Supplementary Video 5). Although not directly relevant to window applications, birefringence reveals nematic-like structures of nanofibre organization with slow spatial changes of nanofibre orientations, which is key to maintaining spatially homogeneous (or slowly varying on scales much larger than the visible wavelength) distribution of the effective refractive index and reducing light scattering associated with such variations<sup>30</sup>.

While the poor mechanical stability of conventional aerogels hinders many technological uses<sup>25,26,42–44</sup>, SiCellA materials are mechanically robust (Fig. 6) with properties partly boosted by silanization. Compressive and flexural deformations reveal that such materials can withstand substantial mechanical loads anticipated during manufacturing and service of various window products (Fig. 6). Periodic cycles of compression reveal no detectable degradation of mechanical performance with time (Fig. 6c and Supplementary Figs. 7 and 8). The films and slabs of SiCellA of millimetre-to-centimetre thickness can be bent and even rolled (Fig. 6c–g and Supplementary Video 6) while retaining high transparency, exhibiting no cracks or degradation of performance. Because the mechanical properties are porosity dependent, the desired mechanical behaviour can be also tuned by preparing samples with different porosities and solid contents (Fig. 6a,b,f). Considering all characteristics described above, SiCellA materials have a

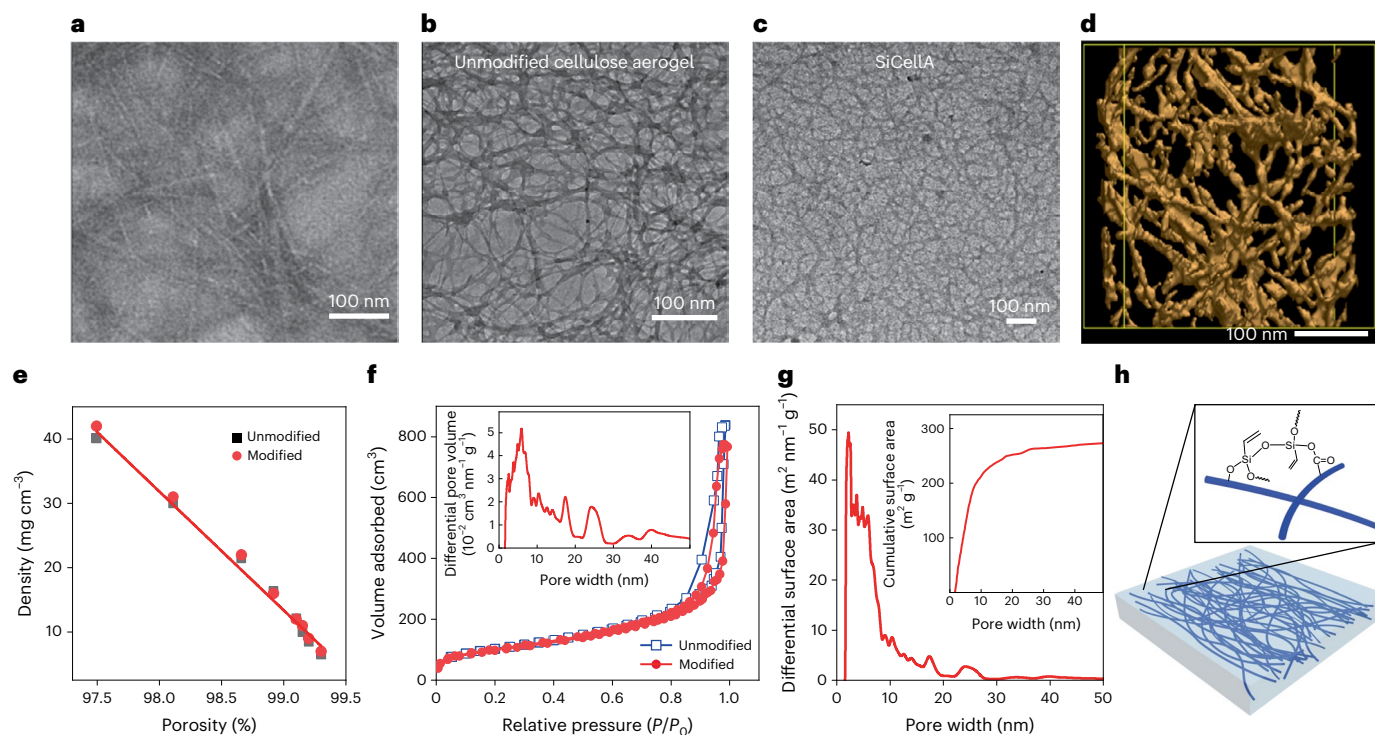


**Fig. 3 | Nanoscale morphology of studied aerogels.** **a, b**, TEM images of ultrasonicated TEMPO-oxidized individual cellulose nanofibres in aqueous dispersions negatively stained with 1% phosphotungstic acid (**a**) and an unmodified nanocellulose aerogel (**b**). **c, d**, TEM image of a silanized aerogel (**c**) and corresponding tomographic TEM visualization of a SiCellA (**d**). **e**, Density of modified and unmodified aerogels depending on porosity. Red line is a guide to the eye. **f**,  $N_2$  adsorption and desorption isotherms for modified and unmodified

aerogels at 77 K. Solid lines connect measured data represented by symbols. The inset shows a distribution of a differential pore volume depending on a pore width for a modified aerogel. **g**, Distribution of a differential pore surface area depending on a pore width for SiCellA. The inset shows a cumulative surface area depending on a pore width. **h**, Schematic diagram of a SiCellA formed by a network of thin cellulose nanofibres (dark blue lines) with silanized surfaces.

unique combination of optical, thermal and mechanical properties that makes them suitable for applications in window products.

## Window products and their durability

There are many stringent requirements for window applications that go well beyond the optical, thermal and mechanical characterizations described above. Some of them are related to durability of materials themselves and the overall glazing products in which these materials are used. The thermogravimetric analysis (TGA), derivative thermogravimetric (DTG) and differential scanning calorimetry (DSC) characterizations of silanized and unmodified cellulose aerogels reveal that they are thermally stable at ambient and elevated temperatures (Fig. 7a,b). Although heating such materials well above 200 °C can cause degradation, no such high temperatures are relevant to window and skylight applications.

The SiCellA aerogels boost the condensation resistance of windows when used both as retrofits and within IGUs (Fig. 7c), with SiCellA-retrofitted single-pane glass showing a condensation resistance factor (CRF) (quantifying the window's ability to resist condensation of water on its surface at low temperatures; Methods) comparable to that of commercial double-pane IGUs<sup>1–9</sup>. A thin double-pane IGU with an air filler replaced by SiCellA shows a CFR of 82, much better than that of 35–50 known for commercial double-pane IGUs<sup>5–9</sup>. As envisaged (Fig. 1a,b), SiCellA substantially boosts the condensation resistance of window products, including single-pane windows upon retrofitting with the aerogel film and IGUs upon inserting the aerogel into the gap of a double-paned IGU (Fig. 7c). There is no detectable performance degradation after the chemical fogging test of a SiCellA IGU (Fig. 7d), which is related to their superhydrophobic nature (Fig. 2h). The fortnight-long 80/80 humidity and ultraviolet exposure

tests reveal no notable/detectable degradation of optical or thermal properties of SiCellA IGUs (Fig. 7e,f). By performing the American Society for Testing and Materials (ASTM) standard tests ASTM 2189 and ASTM 2190-19 (Methods) with the IGU containing SiCellA within its gap, we find no condensation within the interior of the IGU and no notable changes in light transmission and thermal performance in response to chemical processes or factors such as ultraviolet irradiation (Fig. 7d–f and Supplementary Table 2).

To create a robust retrofit product, SiCellAs were adhered to protective clear plastic or thin glass substrates, followed by their lamination atop the inner surfaces of single-pane windows (Fig. 1c,f and Supplementary Fig. 1). The thermal resistance  $R$  value is proportional to a thickness of an insulating material. Therefore, the ensuing  $R$  value of a retrofitted single-pane window then depends on the SiCellA thickness, as we reveal by combining numerical modelling and experimental measurements (Fig. 8a) that involve both real windows and hot/cold box prototypes (Fig. 1f–h and Supplementary Fig. 9). Such boosted-efficiency single-pane windows can now match or exceed the performance of double-paned windows<sup>7</sup> (Fig. 8a). Because the single-pane windows still constitute ~40% of all windows, which is because multi-paned IGUs are often structurally or architecturally incompatible with designs of old, historic buildings, these retrofit products may play an important role in capturing window-related energy losses of pre-existing buildings (Supplementary Fig. 10)<sup>1–4</sup>.

Intended for new construction, the IGUs containing SiCellA can take many different embodiments, where glass panes with or without different low-emissivity coatings can be used, and the thickness of the aerogel filler relative to the overall gap thickness can be varied, along with the thickness of air or other filler gas. The results of numerical modelling for such SiCellA IGUs (Fig. 8b,c) are consistent

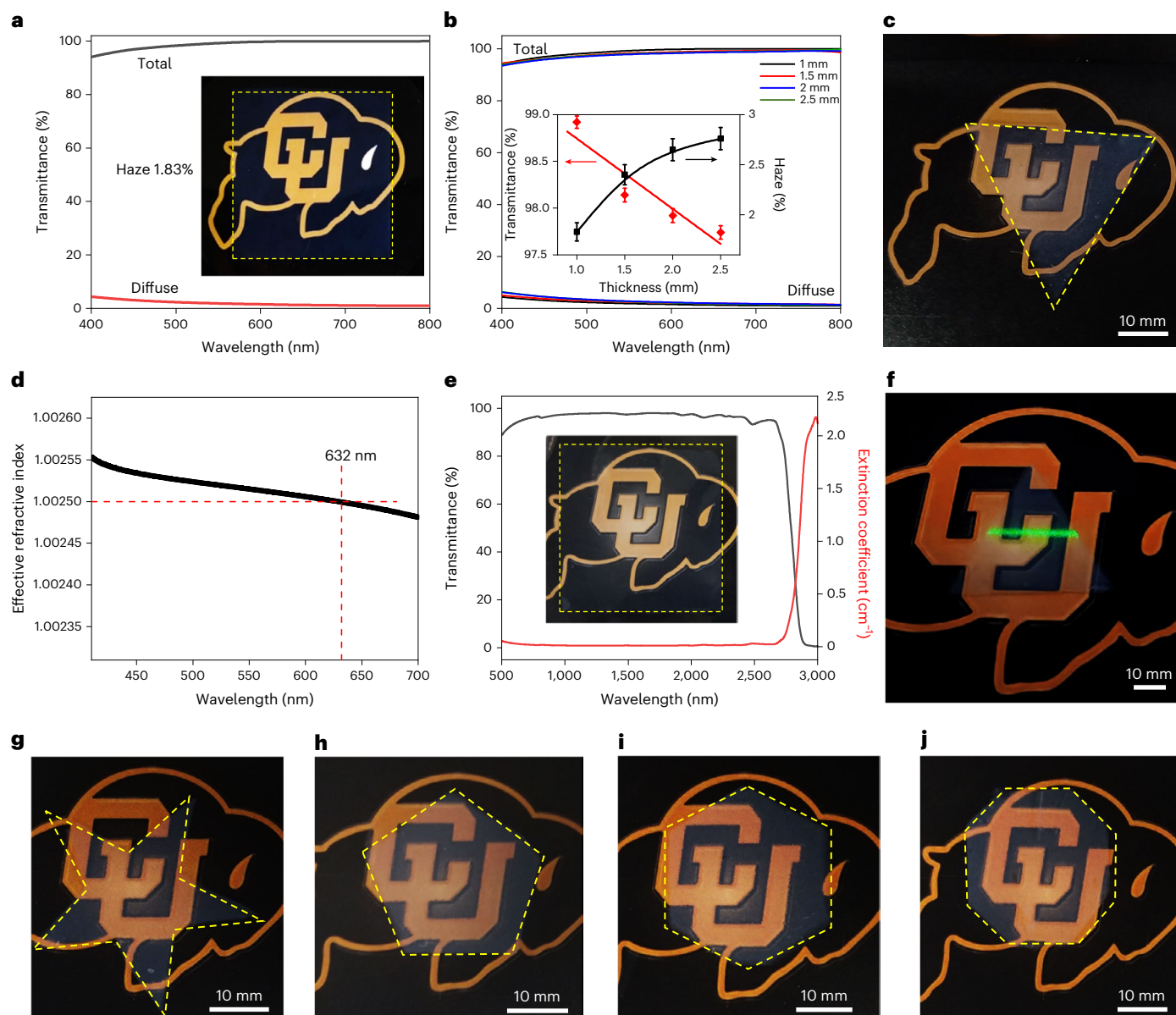


**Fig. 4 | Optical properties of SiCellA materials.** **a, b**, Visible-range spectral dependence of total and diffuse transmittance of 1 mm-thick film shown in the inset (marked by a dashed line) (**a**) and SiCellA films of different thicknesses (**b**). The inset in **b** shows the transmittance and haze depending on SiCellA film thickness with experimental data points represented by symbols with error bars, and solid lines are guides to the eye. Error bars denote the standard deviation from eight independent samples. Data are presented as mean values  $\pm$  standard deviation. **c**, Triangular SiCellA prism with a thickness of 5 mm. **d**, Spectral dispersion of a refractive index as calculated from absorption measurements

using the Kramers–Krönig relations. Dashed lines mark a refractive index of 1.0025 determined at 632 nm by measuring a minimum deviation angle of a laser beam. **e**, Visible through near-infrared spectral dependence of transmittance and extinction coefficient for a 2 mm-thick SiCellA film shown in the inset. **f**, Twenty-five mm-thick SiCellA prism with a 532 nm laser beam passing through without deviation because of its refractive index being close to that of air. **g–j**, Four mm-thick SiCellA prisms with shapes of a star (**g**), a pentagon (**h**), a hexagon (**i**) and an octagon (**j**).

with experimental measurements performed for a set of prototypes that we manufactured (Fig. 8d,e), revealing that the general principles commonly applied to designing glass-based multi-pane IGUs can be adequately adapted to using SiCellA panes and fillers. By using krypton or argon to fill parts of the gap of SiCellA-containing IGUs, when the aerogel fills only part of the gap, the  $R$  values can be boosted further (Fig. 8f and Supplementary Table 3). Adding SiCellA to window products does not degrade optical properties of the overall IGUs (Fig. 8g,h and Supplementary Figs. 1 and 2) because the transmission of SiCellA is very high so that the transmission light losses mainly come from glass and different coatings on it. In terms of this, SiCellAs

are great candidates for the mid panes of IGUs because they allow for higher-than-glass transmission, so that IGUs with large numbers of mid panes can be developed while retaining high overall transmission (Fig. 8g,h and Supplementary Figs. 1 and 2).

## Discussion

Modestly transparent cellulose<sup>25,27,31</sup>, silica<sup>20,23,45</sup>, organic–inorganic hybrid and other aerogels<sup>26,28,29,43</sup> have been demonstrated over the past decades<sup>14,15,17,20,30</sup>, attracting initial interest, but many remaining challenges associated with stringent requirements of glazing products hindered their mainstream applications in windows, skylights and

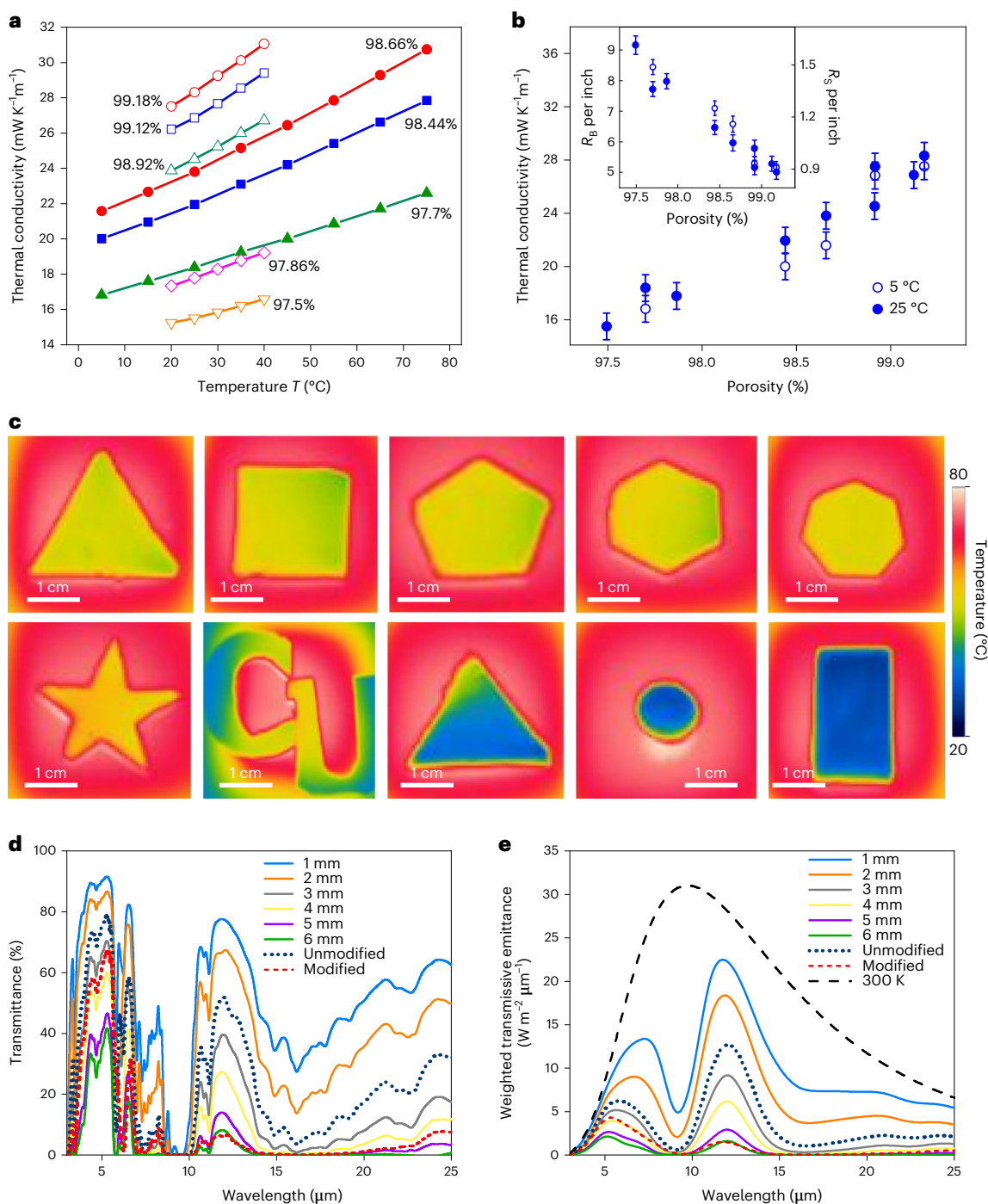


**Fig. 5 | Thermal properties of SiCella.** **a**, Temperature dependence of thermal conductivity of SiCella at different porosities. Solid lines are guides to the eye. **b**, Thermal conductivity dependence on SiCella porosity at 5  $^{\circ}\text{C}$  and 25  $^{\circ}\text{C}$ . The inset shows a dependence of  $R$  per inch on porosity of SiCella:  $R_{\text{S}}$  and  $R_{\text{B}}$  show  $R$  values, respectively, in SI and Imperial units. Symbols with error bars show experimental data points. Error bars denote the standard deviation from five independent samples. Data are presented as mean values  $\pm$  standard deviation. **c**, Infrared thermal images of SiCella films of different shapes placed on a hot

plate: (from top left to bottom right) 4 mm-thick triangle, square, pentagon, hexagon, heptagon, star, University of Colorado logo, 8 mm-thick triangle, 10 mm-thick disc and rectangle. Temperature is coded according to a colour scale. **d**, **e**, Raw infrared transmittance (**d**) and averaged infrared transmissive emittance weighted by 300 K black-body radiation (**e**) of unmodified cellulose-based aerogels at various thicknesses (solid lines). For comparison, spectra for silanized and unmodified aerogels of the same 2.5 mm thickness (red dashed and dark blue dotted lines, respectively) are provided.

other parts of building envelopes. Many aerogels referred to as ‘transparent’, including our previously developed cellulose–polysiloxane hybrid aerogels<sup>19</sup>, do not meet stringent requirements for applications in IGUs because of the relatively large haze values caused by the large fraction of transmitted light being forward scattered. Our work overcomes these major challenges as follows: (1) mechanically robust,

crack-free monolithic SiCella was demonstrated at window-relevant square-metre scales; (2) low haze and high transparency of SiCella meet the requirement of applications in windows; (3) silanization enables super-hydrophobicity of SiCella, making it durable; (4) adhesion of SiCella to glass and plastic films enables its utility in many glazing products and (5) simple fabrication steps, including ones compatible

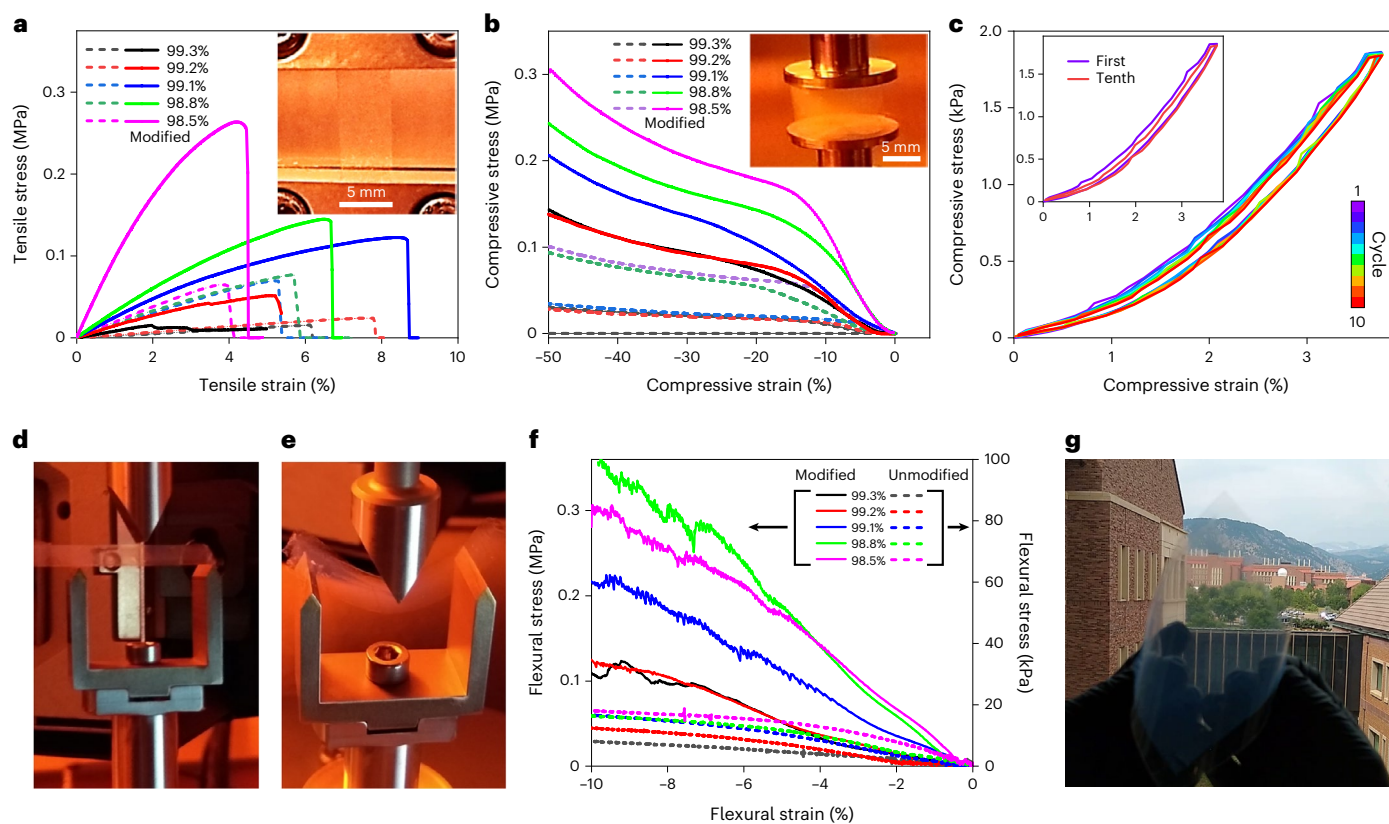


**Fig. 6 | Mechanical properties of cellulose-based aerogels.** **a**, Tensile stress–strain dependence of silanized (solid lines) and unmodified (dashed lines) aerogels with different porosities. The inset shows a SiCellA sample held between tensile mechanical clamps during measurements. **b**, Compressive stress–strain dependence of aerogels with different porosities. The inset shows a SiCellA sample held between compressive mechanical clamps during measurements. **c**, Compressive cycle loops of ten cycles, with a number of a cycle represented by

colours according to a colour scale. The inset shows compressive stress–strain plots for the first and tenth cycles. **d, e**, A SiCellA sample placed on the three-point clamps (**d**) and three-point bending of the SiCellA sample (**e**). **f**, Flexural stress–strain dependence for a 25 mm × 5 mm × 3 mm aerogel sample. Left y axis refers to the silanized SiCellA samples while the right y axis refers to the unmodified SiCellA aerogels. **g**, A photograph of a bent/folded 2 mm-thick aerogel film of 100 mm × 100 mm area showing its rubber-like flexibility.

with roll-to-roll processing, and low-cost source materials (Supplementary Note 1) will help with the deployment.

The fundamental difference of SiCellA as compared with conventional aerogels is that the size of <100 nm pores and <10 nm diameter of nanofibres forming the network (Fig. 3) is controlled to be much smaller than the visible light wavelengths uniformly on window-relevant (square-metre) scales, assuring high visible-range light transmission 97–99% (much better than ~92% transmission of generic clear glass) and haze ~1%. These lightweight materials with mass density ~1% of glass density are mechanically robust to take forms of free-standing films that exhibit thermal conductivity lower than that of still air (Fig. 5). SiCellA can be manufactured at a relatively low cost (Supplementary Note 1) and in a scalable way, promising to enable entirely different types of IGU, skylight, daylighting and even SiCellA-containing window frame design. The abundant source material, which is the wood pulp in the present study, can also be derived from waste of food- and beer-production industries<sup>46–48</sup> with the help of bacteria, with the cost of the end SiCellA film on the order of US\$1 per square foot in both cases (Supplementary Note 1). Additionally, the solar gain control can be potentially done with reflective cholesteric filters based on nanocellulose<sup>49–51</sup>.

Costs and scaling challenges associated with critical-point drying (CPD) are known obstacles for deploying aerogels, with alternative approaches of ambient drying being actively developed (including ones with optical transparency)<sup>52,53</sup>. However, the ability of using rolled aerogel films within the CPD-based drying process, along with pump-less operation and solvent drying mitigates this problem for SiCellA

while yielding superior optical properties. While specific economically viable technical solutions for manufacturing of installation-ready window products still need to be developed, similar to the case of non-transparent aerogels used in pipe insulation and recently even in some parts of building envelopes, the ability of rolling during different stages of aerogel manufacturing may help lowering manufacturing costs and, thus, also market penetration.

Deployment of SiCellA could increase the use of glazing in building envelopes because the aerogel-enhanced windows can exceed current and near-future targets for *R* values of glazing. The low mass density is a key for structural compatibility and retrofitting old windows and for unconventional multi-pane IGU designs. SiCellA's combination of very high transparency and low thermal conductivity at the scale of building materials is a breakthrough, which opens unique opportunities in harnessing and controlling solar energy delivered to buildings, depending on climate- and season-related needs. The boosted performance of SiCellA-based IGUs is directly linked to low thermal conductivity and high visible transmission of these materials when used as the middle panes of IGUs. The reflection coefficient at the air–SiCellA interface is approximately ten times lower than at the glass–air interface, so that multi-pane assemblies with SiCellA-based middle panes exhibit lower light loss due to reflections as compared with their standard counterparts. For a quadruple-pane IGU assembly, for example, the light loss can be reduced by ~16% upon replacing two middle glass panes with SiCellA counterparts (Fig. 8). Each additional SiCellA pane reduces light transmission by less than 1% so that, hypothetically, even ten-pane IGUs can be possible (not possible for glass mid panes as a glass-based

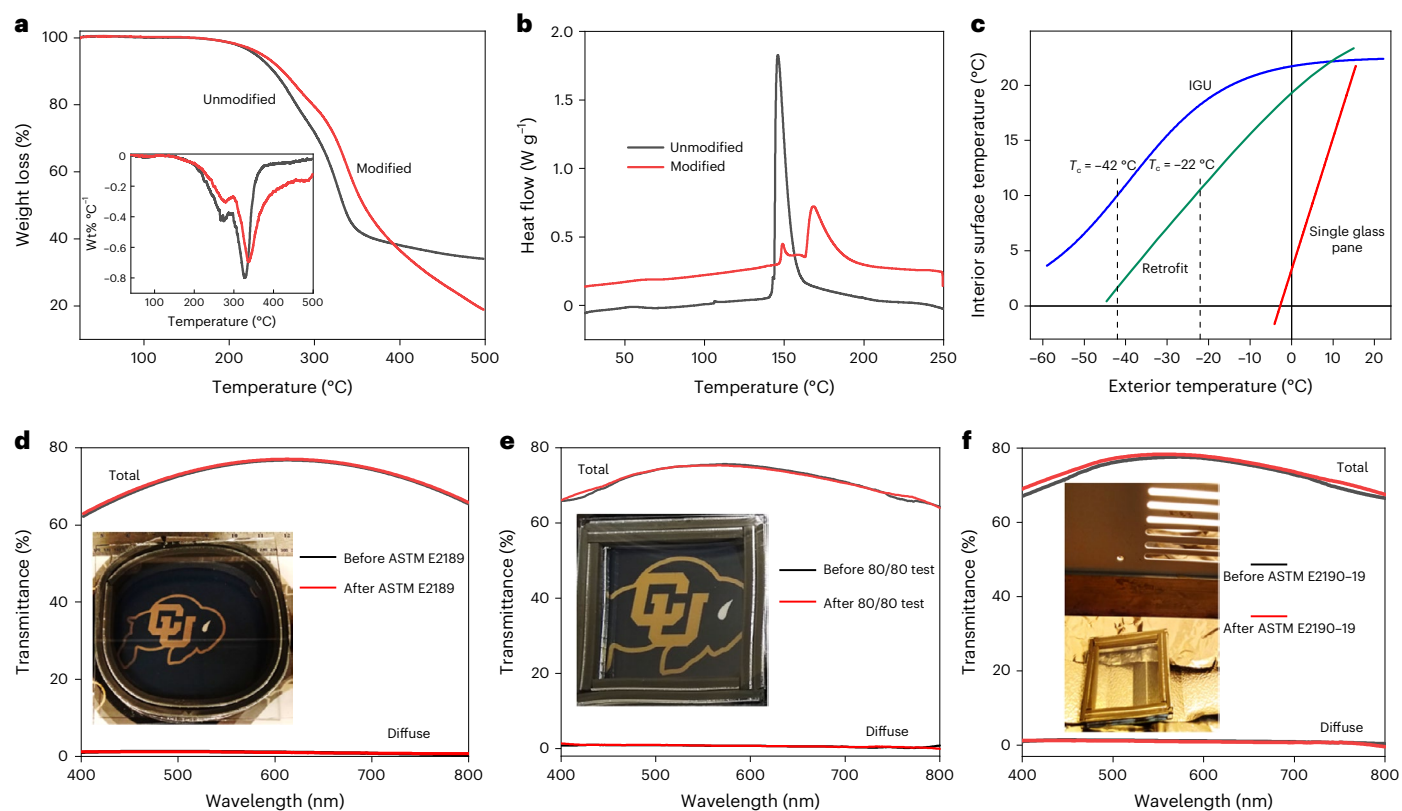


**Fig. 7 | Durability, stability and condensation resistance of SiCellA and window products.** **a**, TGA of silanized and unmodified nanocellulose aerogels showing the percentage of weight loss depending on temperature. The inset shows a DTG analysis of a TGA. **b**, DSC of unmodified and silanized nanocellulose aerogels. **c**, Dependence of an interior surface temperature on exterior temperature for SiCellA-based window products compared with a single glass pane.  $T_c$  (marked by dashed vertical lines) shows the outside temperature when condensation forms on the interior surface of the glass at an interior RH of 50%.

Solid vertical and horizontal lines correspond to zero temperatures; they are axes. **d–f**, Optical performance of a triple-pane IGU with a 3 mm-thick SiCellA layer in the middle before and after a chemical fogging test (**d**), 80/80 durability analysis (**e**) and 30 days of 500 W ultraviolet irradiation analysis (**f**). The insets in **d–f** show, respectively, a 15 cm × 15 cm IGU after the chemical fogging test (**d**), 10 cm × 10 cm IGU after the 80/80 durability test (**e**) and a 10 cm × 10 cm IGU in a chamber under ultraviolet irradiation (**f**).

ten-pane IGU prevents nearly all light from passing due to reflections at 20 interfaces).

In SiCellA-based IGUs, panes can be separated by gaps of a thickness varying within 6–16 mm, which can be optimized depending on a gas filler (Fig. 8b–f and Supplementary Table 3). For example, with ~3 mm outer glass and mid-layer SiCellA panes, a triple-pane IGU can be made to have ~21 mm overall thickness of a standard double-pane IGU to replace one while providing much better insulation at comparable optical transmission. Designs of IGUs can mix free-standing SiCellA mid-layers and ones adhered to glass panes on their inner surfaces. With thermal conductivity lower than ~26 mW K<sup>-1</sup> m<sup>-1</sup> of still air and no convective transfer, the SiCellA-based IGUs can allow for better insulation per inch of a material than a regular double-pane window with an air gap<sup>7</sup> (Fig. 8 and Supplementary Figs. 1 and 2). Low-emissivity coatings can be applied to glass surfaces, such as the inner surface of the exterior glass pane (Fig. 8), though the low-emissivity coatings provide a smaller additional boost of insulation for SiCellA-based IGU assemblies with intrinsic  $R_s > 1.6 \text{ m}^2 \text{ K W}^{-1}$  ( $R_B > 9 \text{ h ft}^2 \text{ °F Btu}^{-1}$ ).

Although the initial deployment of SiCellA-based glazing products will probably focus on conventional windows, SiCellA can also be designed to be translucent and with backscattering for other glazing uses, such as skylights and privacy windows, in which case SiCellA can be deliberately made hazier. High  $R$  values will be attractive for integration of SiCellA-based IGUs with electrochromic and other technologies for privacy and solar gain control<sup>33,34,36</sup>, especially in the multi-pane IGU designs (Fig. 8), so that all-in-one solutions for high energy efficiency

can be realized. The SiCellA-enabled glazing may allow the building envelopes to better take advantage of external conditions while providing natural occupant comfort and potentially even harnessing energy from the environment.

## Conclusions

In summary, we demonstrate scalable manufacturing of highly transparent silanized cellulose aerogels, called SiCellAs, for glazing applications. SiCellA films can be used as IGU fillers and in multi-pane IGU designs to replace the inner glass panes and are fully compatible with the existing solutions for thermal-range emissivity and solar gain control. The market penetration of SiCellA-based products will depend on the ability to manufacture them at low cost, which will require further research and development.

## Methods

### Source materials and oxidation of cellulose

Never-dried hardwood cellulose pulp was obtained from Nine Dragons Paper (Rumford Division). This hardwood kraft pulp with a water content of 92% had been kept in a wet stage after the bleaching treatment. The pulp was demineralized by stirring it in an HCl (0.1 M) solution for 1 h, after which it was washed with deionized (DI) water by filtration and then stored at 4 °C without drying. The TEMPO oxidation of the cellulose pulp was started in a basic medium with a pH of 10 (Supplementary Fig. 3d,e). TEMPO (28.92 mg, 0.094 mmol) and NaBr (317.64 mg) were added to the suspension, followed by addition of 1 M NaOCl solution (10 ml).

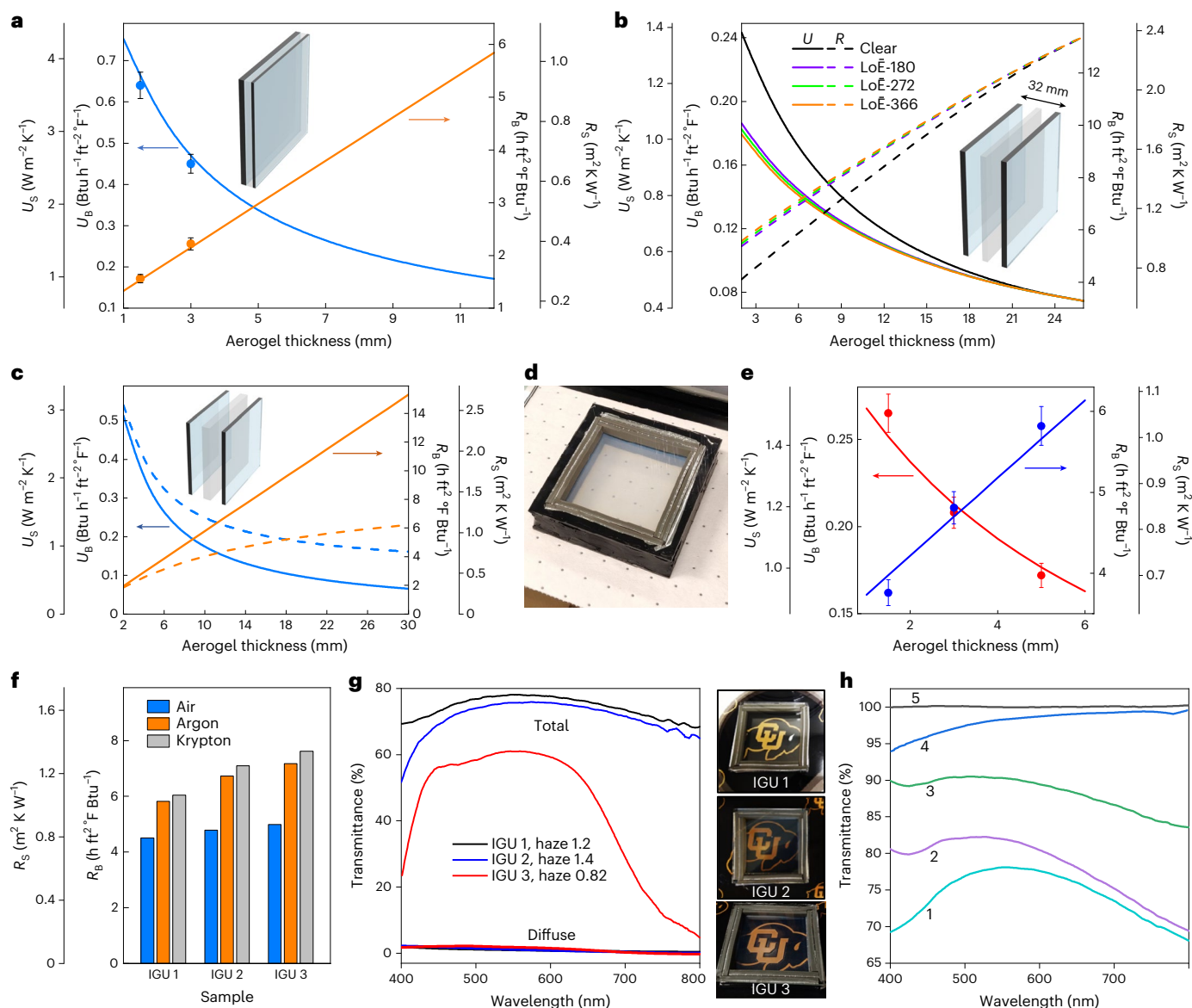


**Fig. 8 | Windows products containing SiCellA.** **a**,  $U$  and  $R$  values for a single-pane window retrofitted with SiCellA of varying thickness on a 100  $\mu\text{m}$ -thick supportive substrate attached to a glass pane (inset schematic); lines and symbols, respectively, show calculated and measured data.  $U_s$  and  $U_b$  show  $U$  values, respectively, in SI and Imperial units. Error bars denote the standard deviation from nine independent samples. Data are presented as mean values  $\pm$  standard deviation. **b**,  $U$  and  $R$  values versus aerogel thickness calculated for a triple-pane IGU of a fixed total thickness of 32 mm and SiCellA used instead of a middle-pane layer and a low-emissivity coating on one of the glass panes. **c**,  $U$  and  $R$  values versus SiCellA thickness calculated for a triple-pane IGU with a SiCellA film in the middle and a 12 mm gap between a glass pane and SiCellA. Solid and dashed lines are calculated for 0% and 16% of average thermal-range infrared transmittance, respectively. **d**, A photograph of fabricated triple-pane 15 cm  $\times$  15 cm IGU with 3 mm-thick SiCellA film used as a middle pane and air

gaps between glass panes and SiCellA fixed at 12 mm. **e**, Calculated (lines) and measured (symbols)  $U$  and  $R$  for a triple-pane IGU shown in **d**. Error bars denote the standard deviation from three independent measurements. Data are presented as mean values  $\pm$  standard deviation. **f**, Calculated  $R$  values for triple-pane IGUs with 3 mm-thick SiCellA film used as a middle pane and two clear glass panes (IGU 1) or one clear glass pane and LoE-180 (IGU 2) or LoE-366 (IGU 3) coating filled with air, argon and krypton. **g**, Spectral dependence of total and diffuse transmittance of triple-pane IGUs with 3 mm-thick SiCellA film used as a middle pane. Right-side inset shows photographs of corresponding IGUs. **h**, Spectral dependence of total visible transmittance of a triple-pane IGU with 3 mm-thick SiCellA between two 3 mm-thick clear glass panes and air gaps of 14 mm (1), double-pane IGU with two clear glass panes of 3 mm thickness and 31 mm air gap (2), 3 mm-thick glass pane retrofitted with 2 mm-thick SiCellA (3), 2 mm-thick free-standing SiCellA (4) and air (5).

When the pH drop was less than 0.01 per minute, the solution was transferred to a blender and blended for several minutes with a relative centrifugal force of 300 g (at 1,500 r.p.m.) (Supplementary Fig. 3f). This breaks down the cellulose fibre agglomerates and allows deeper penetration of the oxidation agent. After a total blending time of 15 minutes, the solution was placed back on a stirring plate and the pH was again adjusted to 10. This process was repeated until the pH of the solution drops less than 0.5 after blending. When the pH of

the solution dropped less than 0.03 in one hour, the reaction was considered finished. The solution was then centrifuged at 10,800 g (9,000 r.p.m.) for 20 minutes to filter the excess chemicals out of the cellulose solution. This process was repeated several times, each time replacing the waste liquid with DI water to remove the remaining chemicals from the solution until only pure, oxidized cellulose fibres remained. The oxidized nanocellulose was then recovered by centrifugation and washed thoroughly with DI water, which was

then mechanically ground with a 1,500 W grinder (Supplementary Fig. 3g), followed by sonication with Branson Sonifier for 15 min at 30% amplitude. Oxidation of the unreacted C6 hydroxyl groups of cellulose into C6 carboxylate groups was further performed using NaClO<sub>2</sub> as the primary oxidant, with catalytic amounts of TEMPO and NaClO in water at a pH of 4.8–6.8. TEMPO again allowed for the selective and efficient conversion of the C6 hydroxyl groups. One M dibasic sodium phosphate (2.35 ml) and 1 M monobasic sodium phosphate (2.65 ml) solutions were added to 1 g TEMPO-oxidized cellulose nanofibre solution (Supplementary Fig. 3h) to act as a buffer during the reaction. This was stirred at 15 g (500 r.p.m.) for approximately 5 minutes and then 20 ml was removed and set aside to dilute the sodium hypochlorite later before adding it to the reaction vessel. TEMPO (25 mg) and sodium chlorite (1.13 g) were then added to the oxidized cellulose nanofibre dispersions and were stirred at 15 g (500 r.p.m.) for approximately 20 minutes until these additives were fully dissolved. Sodium hypochlorite (0.455 ml) was then added to the 20 ml separate solution. The diluted sodium hypochlorite was then added to the cellulose nanofibres dispersion, and the reaction vessel was immediately sealed. The solution was placed in a water bath at room temperature and stirred at 15 g (500 r.p.m.) for approximately 30 minutes. The water bath was then heated to 60 °C and the reaction was allowed to run continuously for 72 h. The solution was centrifuged at 10,800 g (9,000 r.p.m.) for 20 minutes to filter the excess chemicals out of the cellulose solution. This process was repeated several times, each time replacing the waste liquid with DI water to wash out the remaining chemicals until only pure, oxidized cellulose fibres remained. Next, the dispersion was sonicated with a Branson Sonifier for 30 minutes and filtered with Whatman filter paper 2 to get the final oxidized cellulose nanofibre dispersion in water.

### Preparation of aerogels

Aqueous TEMPO-oxidized cellulose nanofibre dispersions with concentrations ranging from 0.5% to 2% were poured into plastic moulds of desired thickness ranging from 1 mm to 25 mm (Supplementary Fig. 4a,b). To initiate gelation, 0.5 M HCl was sprayed into the dispersion for a few seconds with a fine spray. Keeping the sprayed HCl spread over the dispersion, it was allowed to stand for 30 min without any disturbance. The resulting hydrogel was then moved to a 0.1 M HCl solvent bath for 24 h to make sure that the gelation is complete. The ensuing rigid hydrogel was taken from the mould, and the acid was then washed out by DI water and moved to a water–ethanol mixture (50 vol% each) followed by the solvent exchange to ethanol (Fig. 2a and Supplementary Fig. 4b–d). Because the ethanol makes azeotrope with water, we used an elevated temperature of 60 °C during the water-to-ethanol exchange (Supplementary Fig. 4c,d). The ensuing alcogel is then rolled and moved to a CPD chamber to dry (Supplementary Fig. 4g and Supplementary Fig. 5a–c), with the initial chamber temperature and pressure set at 5 °C and 800 psi (pound per square inch), respectively. The next step involved purging ethanol from the chamber and replacing it with liquid CO<sub>2</sub>. Then, the temperature was raised to 40 °C and the pressure was set at 1,500 psi, and the ethanol leftover was purged while within the supercritical phase for 30 min. The final step of the process, bleeding of supercritical CO<sub>2</sub>, was then started slowly, at 25 psi min<sup>-1</sup>, and the chamber was gradually depressurized within about 1 h. The resulting aerogels were kept at 60 °C for 1 day before characterization and functionalization (Supplementary Fig. 4i,h). CPD chambers with cylinder-shaped inner volume of two different dimensions were used (diameter × height sizes of 16.5 cm × 2.5 cm and 16.5 cm × 10.4 cm), depending on the size of SiCellA being dried (Supplementary Figs. 4g–k and 5c–f). Additional details on CPD drying while recycling solvents via pumpless operation are provided in Supplementary Note 2. We also note that a slightly modified fabrication procedure as compared to what is described above can involve first rolling the gel on the plastic support in its hydrogel state while using spacers and then doing solvent

exchanges in cylindrical containers before again obtaining a rolled alcogel for CPD drying.

### Silanization of dried aerogels

Chemical vapour deposition of 1H,1H,2H,2H-Perfluorooctyltriethoxysilane (PFOES) on the unmodified TEMPO-oxidized aerogels was done to transform the amphiphilic cellulose to the one with the hydrophobic surface via silane functionalization of the cellulose nanofibres. The unmodified TEMPO-oxidized cellulose nanofibre aerogel was placed on the top of a Teflon mesh supported with a stainless steel mesh. It was then placed in the middle of a 3 l clear polycarbonate vacuum desiccator with the sample thus suspended to functionalize through the interaction with the vapour-phase (Supplementary Fig. 11a) silane molecules. Liquid PFOES (1 mmol g<sup>-1</sup> of unmodified aerogel) was previously placed inside the lower part of the desiccator with a 5 ml Teflon PTFE beaker. The desiccator was sealed, evacuated and moved into an oven which was preheated to 95–99 °C while keeping the temperature below 100 °C (temperatures above 100 °C were observed to reduce transmittance of the silanized aerogel). The reaction time and temperature depend on the thickness of the unmodified aerogel sample (Supplementary Fig. 11b), which was optimized based on repeated test experiments<sup>54</sup>. PFOES molecules undergo hydrolysis and chemical condensation reactions with unmodified TEMPO-oxidized cellulose nanofibres for grafting.

The desiccator was then removed from the oven and allowed to cool down to room temperature. Nitrogen gas was flushed into the cooled desiccator to release the vacuum. The resulting superhydrophobic aerogel inside the desiccator was purged once again with more nitrogen gas to clean the aerogel with inert gas. The effectiveness and universality of the silane functionalization on thick samples were examined with probing transmittance infrared spectra and water contact angle measurements (Fig. 2g,h). The modified aerogels were kept in the oven at 50 °C for 24 h of further characterizations and application. Most commonly (and for all SiCellA samples characterized in Figs. 1–8), silanization of cellulose molecules was done after fabricating aerogels, as depicted in Fig. 2f and Supplementary Fig. 4g–k, though modification at the hydrogel stage can be also done (Fig. 4e,f,h). Uniformity and universality in optical properties of a square-metre SiCellA sample (2 mm thick) were analysed for randomly selected 20 sample areas from the different regions of the aerogel. The summary of the 20 measurements of transmittance is provided in Supplementary Fig. 11c. The obtained superhydrophobic SiCellA materials (Fig. 2h and Supplementary Video 1) exhibited the desired physical properties, comparable to or better than unmodified cellulose aerogels, as detailed below.

The mechanical and optical properties of the SiCellA are strongly influenced by silanization. The synergetic effect of silanization and nanoporous structural design resulted in an optimized elasticity and optical properties of SiCellA. The silanized aerogels exhibited enhanced mechanical performance (200–300% of the increase in tensile and compressive stress of SiCellA than unmodified aerogel), with modified nanoscale porous structure also achieved through silanization (Fig. 3). The SiCellA has higher values of tensile stress (270 kPa) and strain (8.8%) than their corresponding unmodified counterparts (Fig. 6a,b,f). The ultimate compressive stress of the SiCellA is 1.5 MPa, which is three times higher than the respective unmodified aerogel. The enhanced interaction of the silanized cellulose chains within the network after silanization resulted in a substantial increase in deformation resistance, ductility and toughness of SiCellA (Fig. 6). No notable difference was detected in optical properties of the SiCellA and unmodified cellulose aerogels for the studied samples prepared under optimized conditions. The silanization process makes nanocellulose-based aerogels fire retardant and not flammable, meaning that they do not ignite or burn when exposed to an open flame, though they can be damaged and eventually destroyed by the open fire.

### Hydrogel-stage silanization

As an alternative to modifying dried aerogels, silanization was also done at the hydrogel stage, yielding similar results in terms of aerogel properties. In this case, the silanization of cellulose molecules of the fabricated hydrogel was done using vinyltrimethoxysilane as the coupling agent (Supplementary Fig. 4e–h). The fabricated TEMPO-oxidized cellulose hydrogels were dipped in a circulating bath of ethanol/water mixture at the 60:40 ratio with the optimized concentration (5%) of the coupling agent for 4 h (ref. <sup>55</sup>). To ensure efficient coating of vinyltrimethoxysilane coupling agent on the individual exposed cellulose nanofibres, the pH of the solution was maintained between 3.5 and 4 by using the METREPAK Phydriion buffers<sup>55</sup>. Afterwards, the ethanol–water mixture was drained out and replaced with pure ethanol by repeated washing. The ensuing silanized TEMPO-oxidized cellulose alcogels were dried in a CPD chamber (Supplementary Fig. 4f–h). The vinyltrimethoxysilane-modified aerogels produced after CPD drying were kept in the oven at 60 °C for 24 h before applying to window applications and further characterizations.

### Thermal characterization

Thermal conductivity,  $k$ , of aerogels was characterized by two methods: using a commercial heat flow meter Netzsch HFM 446 or by measuring the heat flux through the sample using a sensor (FluxTeq), depending on dimensions of the samples. In the former case, the aerogels were prepared with dimensions specified in instrument's guidelines, with lateral size ranging from 10 cm × 10 cm to 20 cm × 20 cm, whereas the latter method was used for samples of sizes from square inch to square metre.

Thermal conductivity of large-area aerogel films and the  $U$  values of SiCellA aerogel prototypes were determined by measuring the heat flux through the samples<sup>56–58</sup>. To study the heat exchange between the interior and exterior environments separated by a window retrofitted with a SiCellA film and to measure its  $U$  value, we have built an environmental hot/cold box apparatus (Supplementary Fig. 9). The overall dimensions of the box were 1.3 m × 1.3 m × 0.5 m, with its insulating double walls built using a commercial polystyrene foam of 38 mm wall thickness and  $R_s \approx 1.8 \text{ m}^2 \text{ K W}^{-1} / R_p = 10 \text{ h ft}^2 \text{ }^\circ\text{F Btu}^{-1}$  (FOAMULARNGX). The hot/cold box could fit samples of different aspect ratio and area up to 1 m<sup>2</sup>. To mimic the heat exchange between the building's interior and the outdoors environment under different conditions, the inside of the box was heated with an electronically controlled heating band or cooled with dry ice. Thus, the internal temperature of the box, which corresponds to the outdoor ambient temperature, could be changed within a wide range of approximately –70 °C to 100 °C. The air temperatures inside,  $T_e$ , and outside,  $T_i$ , the box, and temperatures of the window surfaces were continuously monitored with thermocouples. The heat flux sensor (FluxTeq) was used to measure the heat flux flow,  $q$ , through the measured assembly or IGU. Data from the heat flux sensors and thermocouples were collected by a computer using an automatic data-acquisition software (Supplementary Fig. 9). The heat flow through the characterized SiCellA material, assembly or IGU could be monitored over hours or days, if necessary. This system was used to measure thermal conductivity, thermal conductance,  $U$  and  $R$  values. For example, the  $U$  value of our window retrofitted with an aerogel film or IGU was calculated as<sup>56–58</sup>  $U = 1/R = q / (T_i - T_e)$  using the measured values of  $q$ ,  $T_i$  and  $T_e$ .

### Optical characterization

The ultraviolet through visible and near-infrared spectra were measured by a Cary 500 scan spectrophotometer in transmission mode. The total and diffused transmission spectra in the visible region (400–800 nm) of aerogel films were recorded with an integrating sphere (Labsphere DRA-CA-5500) with an inside diameter of 150 mm and coated with barium sulfate. The haze coefficient values, quantifying the amounts of scattered light, were calculated based on the total and

diffused transmission measurements using the integrating sphere following the ASTM D1003 (Standard Test Method for Haze and Luminous Transmittance), commonly used for haze measurements in windows applications. For optical transmittance and haze measurements, the samples were mounted at the entry port of the integrating sphere and calibration was done using diffuse reflectance standards. The samples, with an area of 10 cm × 10 cm for free-standing, retrofitted samples and 10 cm × 10 cm × 3.6 cm for triple-pane IGUs were normally inserted in the instrument's standard sample compartment. To enable the mounting of these modestly large samples, the standard sample compartment covers were removed and a light-tight customized housing was used.

Fourier-transform infrared spectroscopy experiments were performed in the mid-infrared (2.5–25 μm) region using a Nicolet 6700 Fourier-transform infrared spectrometer with a deuterated triglycine sulfate detector (4,000–400 cm<sup>-1</sup>) in a transmission mode. A gold-coated integrating sphere with a diameter 75 mm (PIKE Technologies, Mid-IR Upward-looking InegratIR) was used in both reflection and transmission modes with a wide-band (4,000–500 cm<sup>-1</sup>) Mercury Cadmium Telluride detector. These measurements allowed for characterizing thermal–infrared-range transmissivity of various unmodified and SiCellA aerogels shown in Fig. 5d. The weighted transmissive emittance ( $W \text{ m}^{-2} \mu\text{m}^{-1}$ ), that is, the ratio of the thermal transmittance from aerogels to the radiation from an ideal black body at the same temperature, were calculated by multiplying black-body emittance at 300 K by the averaged transmittance of aerogels at each wavelength (Fig. 5e). Those data were used as an input for modelling of thermal performance of fabricated glazing products.

The colour appearance of objects seen through materials and IGUs is quantitatively described by a colour rendering index<sup>38,39</sup>. The colour rendering index of SiCellA films and SiCellA IGUs was determined based on light transmission measured by a Cary 500 scan spectrophotometer while following ASTM standards<sup>38,39,59,60</sup> and was found to be >99%, meeting requirements for IGUs.

Optical microscopy observations of hydrogel, alcogel and aerogel samples were performed using an upright Olympus microscope BX-51. A digital camera Nikon D50 mounted on the microscope and small-magnification (2× or 4×) Olympus objectives were used to take photographs of water droplets on the surface of SiCellA films, which allowed for measuring a contact angle and determining surface wettability using ImageJ software (freeware, National Institutes of Health). Refractive index values of SiCellA aerogels were obtained by measuring a minimum deviation angle by a prism made of this material<sup>61–63</sup>, where a laser beam from a 632 nm helium–neon laser (Edmund Optics) was deviated by an aerogel prism placed on a rotating holder (Olympus). By measuring a minimum deviation angle of a beam and a corresponding incidence angle, refractive index values of transparent aerogels were determined with high accuracy<sup>61–63</sup>. Additionally, a spectral dispersion of a refractive index (Fig. 4d) was obtained from the measured absorption data of aerogel films by using the Kramers–Krönig relation<sup>61,64</sup>. To measure optical birefringence in 12 mm-thick aerogel samples with porosity of 99.1%, we used a Berek compensator U-CTB (Olympus) mounted on a microscope in an optical path immediately after a SiCellA sample.

### Mechanical characterization

Tensile mechanical measurements were done using a DMA 850 apparatus (TA Instruments) with a standard tension clamp attachment. The compression, three-point bending and cycles of compression and elongation were recorded using the RSA-G2 Solids Analyser. Initial dimensions of samples were used to convert these measurements to stress and strain with TRIOS software (TA Instruments). Mechanical properties were also probed under cyclic tension/compression up to a maximum strain of 6% for silanized aerogels (Fig. 6c and Supplementary Fig. 8). In each cycle, the stress rose linearly with increasing strain to a maximum value, at which the load was removed and the stress

typically came back to the original value (Supplementary Figs. 7 and 8), indicating no hysteresis behaviour at up to 6% strain on compression and elongation. Below 6% strain, the maximum value of stress remained constant with increasing the cycle number, confirming the overall robust mechanical performance of SiCellA materials (Fig. 6 and Supplementary Figs. 7 and 8).

### Material stability and window product durability

TGA was performed for both unmodified and silanized aerogels in the N<sub>2</sub> atmosphere at 25–500 °C. TGA runs were performed with a Netsch STA 449 F1 Jupiter thermogravimeter with an alumina crucible at a heating rate of 10 °C min<sup>-1</sup> in argon atmosphere. The thermal stability was characterized using a basic mass loss rate,  $dm/dt$ , normalized by the total mass lost. DSC was performed using the Q1000 instrument (TA Instruments) with an aluminium hermetic crucible. All tests were performed in the N<sub>2</sub> environment, with the heating and cooling rates set to 10 °C min<sup>-1</sup> and with temperature ramping between 30 °C and 250 °C for one cycle total.

High relative humidity (RH) environments are common for IGUs, especially when installed in tropical or sub-tropical climate regions. The excessive moisture and oxygen in the air can react, for example, with the secondary silicone sealant, accelerating its ageing process and degrading the performance of the IGU. In our study, a high RH environmental test chamber was used to generate a temperature regime of 80 °F (27 °C) at a high RH of 80%. SiCellA-containing IGUs were placed in the chamber for 14 days. The properties of the IGUs before and after the test were then measured, revealing robust performance (Fig. 7e). The fogging test (also known as a ‘chemical outgassing test’) is intended to determine the resistance of preassembled, sealed IGUs to fogging, which could occur due to chemical outgassing of materials and assembly components within the IGU. The test is conducted for 14 days in a special box equipped with an ultraviolet light source, an air circulating fan and a cooling plate according to the standard ASTM E2189, with the outcomes revealing no degradation of physical properties (Fig. 7d). For the ultraviolet exposure test, the IGUs were placed into the ultraviolet illumination chamber and exposed to a 500 W ultraviolet radiator with the output power of 40 W m<sup>-2</sup> or higher, where the ultraviolet exposure photons have energies comparable to the dissociation energies of polymer bonds (300–1,000 kJ mol<sup>-1</sup>). SiCellA-containing IGUs were kept in the chamber at 50 ± 3 °C for 30 days of exposure and then characterized, revealing no substantial property degradation (Fig. 7f).

### Condensation resistance

Cold temperatures of a window’s inner surface can cause moisture from the interior of a room to condense on it as droplets of water when these temperatures are below the dew point. Being highly likely at high indoor RH, the condensation impacts the transparency of windows and the indoor humidity, which may degrade the indoor air quality. To compare the condensation resistance of SiCellA-based window products and their counterparts, we measured their CRF<sup>65,66</sup>, which quantifies how well a window resists condensation on the interior-facing surface. Typical CRF values are 5–15 for single-pane, 35–50 for double-pane and 60–80 for triple-pane IGUs. To measure CRF, we used a home-built cold box apparatus (Supplementary Fig. 9a). The temperature inside the apparatus, which represents the outside ambient environment and exterior temperature, was lowered using dry ice and the temperatures of all IGU surfaces were continuously monitored by thermocouples (FluxTeq). Figure 7c shows dependencies of the temperature of the interior pane surface on the exterior temperature for different characterized fenestrations. The CFR was calculated as  $CRF = 100 (T_c - T_e) / (T_i - T_e)$ , where  $T_c$ ,  $T_i$  and  $T_e$  are, respectively, the temperature of the IGU’s inner surface facing the room, internal room temperature and external temperature experimentally measured when water condenses on the IGU. Condensation was detected visually and also via measuring

the drop of intensity of a 632 nm laser beam (Edmund Optics) passing through the centre of IGU<sup>66</sup>.

### Nanoscale characterization

Transmission electron microscopy (TEM) characterization was done by recording tilt series on a Titan Krios G3i at 300 kV under low dose conditions. SerialEM was used to record the tilt series and reconstruction of the tomographic data was done using IMOD image processing software<sup>67,68</sup>. The individual cellulose nanofibres within aqueous dispersions were negatively stained with 1% phosphotungstic acid before the TEM imaging using a Tecnai ST20 200 kV (Fig. 3a–d). Thin aerogels were fabricated and dried on 300-mesh Au carbon film TEM grids for imaging to avoid possible changes of the internal structure during transfers and processing.

Characterization of nanoscale porosity of aerogels was also carried out with Nitrogen adsorption–desorption measurements, which were performed on a Quantachrome NOVA touch pore analyser at 77 K. Before these measurements, the aerogel samples (about 50 mg each) were kept at 60 °C for 48 h, outgassed under vacuum at 50 °C for at least 24 h and then squeezed into tube-shaped sample holders. By using ASiQwin software, the specific surface area was calculated based on the Brunauer–Emmett–Teller (BET) multi-point method and then pore-size distribution was evaluated according to the density functional theory models implemented within the instrument’s software. The specific surface area was determined by the BET methods from the linear region of the isotherms in the relative pressure ( $P/P_0$ ) range of 0.03–0.3. The specific surface area and pore-size distribution measurements were evaluated by the density functional theory method. The total pore volumes were estimated from the amount of N<sub>2</sub> adsorbed at  $P/P_0 = 0.99$  for porosities of the studied aerogels ranging within 99.3–97.5%. Adsorption isotherms, total surface area, individual and cumulative pore surface area of the unmodified and silanized aerogel were characterized (Fig. 3f,g and Supplementary Fig. 6).

### Modelling and characterization of SiCellA-based products

Numerical simulations of SiCellA-insulated glazing units (Fig. 8 and Supplementary Table 3) were performed using the Berkeley Lab WINDOW 7.7 software<sup>69</sup> while assuming 1,000 mm by 1,000 mm lateral dimensions and SiCellA’s thermal conductivity of  $-0.014 \text{ W K}^{-1} \text{ m}^{-1}$  (Fig. 5a,b). All spectral characteristics were experimentally obtained using spectrometers, as described above, and then loaded into the user-defined input of the International Glazing Database while using Berkeley Lab Optics 6 for defining optical layers and calculating spectral data<sup>69</sup>. The glass panes were assumed to be made of a generic clear glass (3 mm thick), unless noted differently. For retrofits, either a generic thin glass (0.5 mm thick) or a polyethylene terephthalate film of 0.2 mm thickness was used as back-supporting protective layers of the SiCellA-based retrofit prototypes. For low-emissivity coated glass panes, we used 3 mm-thick LoE-180, 272 and 366 window products of Cardinal Glass Industries, with the physical characteristics available in the International Glazing Database.

### Fabrication of SiCellA-based products

The SiCellA were fabricated and adhered to plastic substrates used as a mould during fabrication and as a protective layer in the retrofit product. Alternatively, free-standing films of SiCellA could be easily electrostatically adhered to glass substrates and plastic support layers during retrofit installation so that only edges of the retrofitted windows needed sealing. For low-emissivity coated glass panes, we used 3 mm-thick LoE-180, 272 and 366 window products of Cardinal Glass Industries. IGUs with different lateral dimensions, ranging from 10 cm × 10 cm to 100 cm × 100 cm, and the number of glass or SiCellA panes were fabricated and experimentally characterized. The 3 mm-thick free-standing SiCellA aerogels were used as the middle panes of SiCellA-based triple-pane IGUs. The gap thickness between

glass and SiCellA panes was defined by spacers from Super Spacer SS1466 Gray Edgetech with 6.3 mm and 12.7 mm width. The boundaries of the IGUs were sealed airtight with Silicone Foam and Metal Spacer I. G. Sealant (C.R. Laurence Co.).

## Data availability

All data generated or analysed during this study are included in the published article and its Supplementary Information and Source Data files. Additional information is available from the corresponding author upon reasonable request. Source data are provided with this paper.

## References

- Lovell, J. *Building Envelopes: An Integrated Approach* (Architecture Briefs) (Princeton Architectural Press, 2010).
- Trubiano, F. *Design and Construction of High-Performance Homes: Building Envelopes, Renewable Energies and Integrated Practice* (Taylor and Francis, 2013).
- Pérez-Lombard, L., Ortiz, J. & Pout, C. A review on buildings energy consumption information. *Energ. Build.* **40**, 394–398 (2008).
- Chung, W. Review of building energy-use performance benchmarking methodologies. *Appl. Energy* **88**, 1470–1479 (2011).
- Carmody, J., Selkowitz, S., Lee, E. S., Arasteh, D. & Willmert, T. *Window Systems for High-Performance Buildings* (W.W. Norton & Company, 2004).
- Bansal, N. K. *Energy Efficient Windows* (Anamaya Publishers, 2006).
- Aguilar-Santana, J. L., Jarimi, H., Velasco-Carrasco, M. & Riffat, S. Review on window-glazing technologies and future prospects. *Int. J. Low-Carbon Technol.* **15**, 112–120 (2020).
- Hart, R., Selkowitz, S. & Curcija, C. Thermal performance and potential annual energy impact of retrofit thin-glass triple-pane glazing in US residential buildings. *Build. Simul.* **12**, 79–86 (2019).
- Manz, H., Brunner, S. & Wullschleger, L. Triple vacuum glazing: heat transfer and basic mechanical design constraints. *Sol. Energy* **80**, 1632–1642 (2006).
- Cuce, E., Young, C. H. & Riffat, S. B. Thermal performance investigation of heat insulation solar glass: a comparative experimental study. *Energy Build.* **86**, 595–600 (2015).
- Aegerter, M. A., Leventis, N. & Koebel, M. M. *Aerogels Handbook* (Springer, 2011).
- Pierre, A. C. & Pajonk, G. M. Chemistry of aerogels and their applications. *Chem. Rev.* **102**, 4243–4266 (2002).
- Baetens, R., Jelle, B. P. & Gustavsen, A. Aerogel insulation for building applications: a state-of-the-art review. *Energy Build.* **43**, 761–769 (2011).
- Rubin, M. & Lampert, C. M. Transparent silica aerogels for window insulation. *Sol. Energy Mater.* **7**, 393–400 (1983).
- Duer, K. & Svendsen, S. Monolithic silica aerogel in superinsulating glazings. *Sol. Energy* **63**, 259–267 (1998).
- Schultz, J. M., Jensen, K. I. & Kristiansen, F. H. Super insulating aerogel glazing. *Sol. Energy Mater. Sol. Cells* **89**, 275–285 (2005).
- Buratti, C. & Moretti, E. Glazing systems with silica aerogel for energy savings in buildings. *Appl. Energy* **98**, 396–403 (2012).
- Gao, T., Jelle, B. P., Ihara, T. & Gustavsen, A. Insulating glazing units with silica aerogel granules: the impact of particle size. *Appl. Energy* **128**, 27–34 (2014).
- Liu, Q. et al. Flexible transparent aerogels as window retrofitting films and optical elements with tunable birefringence. *Nano Energy* **48**, 266–274 (2018).
- Buratti, C., Belloni, E., Merli, F. & Zinzi, M. Aerogel glazing systems for building applications: a review. *Energy Build.* **231**, 110587 (2021).
- Belloni, E., Buratti, C., Merli, F., Moretti, E. & Ihara, T. Thermal-energy and lighting performance of aerogel glazings with hollow silica: field experimental study and dynamic simulations. *Energy Build.* **243**, 110999 (2021).
- Gao, T., Ihara, T., Grynning, S., Jelle, B. P. & Lien, A. G. Perspective of aerogel glazings in energy efficient buildings. *Build. Environ.* **95**, 405–413 (2016).
- Lin, J. et al. A review of recent progress on the silica aerogel monoliths: synthesis, reinforcement, and applications. *J. Mater. Sci.* **56**, 10812–10833 (2021).
- Carroll, M. K., Anderson, A. M., Mangu, S. T., Hajjaj, Z. & Capron, M. Aesthetic aerogel window design for sustainable buildings. *Sustainability* **14**, 2887 (2022).
- Kobayashi, Y., Saito, T. & Isogai, A. Aerogels with 3D ordered nanofiber skeletons of liquid-crystalline nanocellulose derivatives as tough and transparent insulators. *Angew. Chem. Int. Ed.* **53**, 10394–10397 (2014).
- Shimizu, T., Kanamori, K., Maeno, A., Kaji, H. & Nakanishi, K. Transparent ethylene-bridged polymethylsiloxane aerogels and aerogels with improved bending flexibility. *Langmuir* **32**, 13427–13434 (2016).
- Fischer, F., Rigacci, A., Pirard, R., Berthon-Fabry, S. & Achard, P. Cellulose-based aerogels. *Polymer* **47**, 7636–7645 (2006).
- Cai, J. et al. Cellulose–silica nanocomposite aerogels by in-situ formation of silica in cellulose gel. *Angew. Chem. Int. Ed.* **51**, 2076–2079 (2012).
- Hayase, G. et al. Polymethylsiloxane–cellulose nanofiber biocomposite aerogels with high thermal insulation, bendability & superhydrophobicity. *ACS Appl. Mater. Interfaces* **6**, 9466–9471 (2014).
- Smalyukh, I. I. Thermal management by engineering the alignment of nanocellulose. *Adv. Mater.* **33**, 2001228 (2020).
- Zaman, A., Huang, F., Jiang, M., Wei, W. & Zhou, Z. Preparation, properties, and applications of natural cellulosic aerogels: a review. *Energy Built Environ.* **1**, 60–76 (2020).
- Davy, N. C. et al. Pairing of near-ultraviolet solar cells with electrochromic windows for smart management of the solar spectrum. *Nat. Energy* **2**, 17104 (2017).
- Strand, M. T. et al. Polymer inhibitors enable >900 cm<sup>2</sup> dynamic windows based on reversible metal electrodeposition with high solar modulation. *Nat. Energy* **6**, 546–554 (2021).
- Islam, S. M., Hernandez, T. S., McGehee, M. D. & Barile, C. J. Hybrid dynamic windows using reversible metal electrodeposition and ion insertion. *Nat. Energy* **4**, 223–229 (2019).
- Fukuzumi, H., Tanaka, R., Saito, T. & Isogai, A. Dispersion stability and aggregation behavior of TEMPO-oxidized cellulose nanofibrils in water as a function of salt addition. *Cellulose* **21**, 1553–1559 (2014).
- Isogai, A., Saito, T. & Fukuzumi, H. TEMPO-oxidized cellulose nanofibers. *Nanoscale* **3**, 71–85 (2011).
- Liu, Q. & Smalyukh, I. I. Liquid crystalline cellulose-based nematogels. *Sci. Adv.* **3**, e1700981 (2017).
- Hunt, R. W. G. & Pointer, M. R. *Measuring Colour* 4th edn (John Wiley & Sons, 2011).
- Dangol, R., Krusselbrink, T. & Rosemann, A. Effect of window glazing on colour quality of transmitted daylight. *J. Daylighting* **4**, 37–47 (2017).
- Lu, X. & Arduini-Schuster, M. C. Thermal conductivity of monolithic organic aerogels. *Science* **255**, 971–972 (1992).
- Apostolopoulou-Kalkavoura, V., Munier, P. & Bergström, L. Thermally insulating nanocellulose-based materials. *Adv. Mater.* **33**, 2001839 (2021).
- Plappert, S. F., Nedelec, J. M., Rennhofer, H., Lichtenegger, H. C. & Liebner, F. W. Strain hardening and pore size harmonization by uniaxial densification: a facile approach toward superinsulating aerogels from nematic nanofibrillated 2,3-dicarboxyl cellulose. *Chem. Mater.* **29**, 6630–6641 (2017).

43. Hasegawa, G. et al. Highly flexible hybrid polymer aerogels and xerogels based on resorcinol-formaldehyde with enhanced elastic stiffness and recoverability: insights into the origin of their mechanical properties. *Chem. Mater.* **29**, 2122–2134 (2017).
44. Kanamori, K. & Nakanishi, K. Controlled pore formation in organotrialkoxysilane-derived hybrids: from aerogels to hierarchically porous monoliths. *Chem. Soc. Rev.* **40**, 754–770 (2011).
45. Pajonk, G. M. Transparent silica aerogels. *J. Non-Cryst. Solids* **225**, 307–314 (1998).
46. Brown, R. M., Willison, J. H. & Richardson, C. L. Cellulose biosynthesis in *Acetobacter xylinum*: visualization of the site of synthesis and direct measurement of the in vivo process. *Proc. Natl Acad. Sci. USA* **73**, 4565 (1976).
47. Repula, A., Abraham, E., Cherpak, V. & Smalyukh, I. I. Biotropic liquid crystal phase transformations in cellulose-producing bacterial communities. *Proc. Natl Acad. Sci. USA* **119**, e220093011 (2022).
48. Fleury, B. et al. Aerogel from sustainably grown bacterial cellulose pellicles as a thermally insulative film for building envelopes. *ACS Appl. Mater. Interfaces* **12**, 34115–34121 (2020).
49. Liang, H. L. et al. Roll-to-roll fabrication of touch-responsive cellulose photonic laminates. *Nat. Commun.* **9**, 4632 (2018).
50. Fernandes, S. N. et al. Cellulose nanocrystals: mind the microgap in iridescent cellulose nanocrystal films. *Adv. Mater.* **29**, 1603560 (2017).
51. De La Cruz, J., Liu, Q., Frazier, A. W., Senyuk, B. & Smalyukh, I. I. Cellulose-based photonic structures as optical filters and solar gain regulating films. *ACS Photonics* **5**, 2468–2477 (2018).
52. Shimizu, T. et al. Transparent, highly insulating polyethyl- and polyvinylsiloxane aerogels: mechanical improvements by vulcanization for ambient pressure drying. *Chem. Mater.* **28**, 6860–6868 (2016).
53. Shimizu, T., Kanamori, K. & Nakanishi, K. Silicone-based organic-inorganic hybrid aerogels and xerogels. *Chem. Eur. J.* **23**, 5176–5187 (2017).
54. Tejado, A., Chen, W. C., Alam, M. N. & van de Ven, T. G. M. Superhydrophobic foam-like cellulose made of hydrophobized cellulose fibres. *Cellulose* **21**, 1735–1743 (2014).
55. Thakur, M. K., Gupta, R. K. & Thakur, V. K. Surface modification of cellulose using silane coupling agent. *Carbohydr. Polym.* **111**, 849–855 (2014).
56. Tritt, T. M. *Thermal Conductivity: Theory, Properties, and Applications* (Kluwer Academic/Plenum Publishers, 2004).
57. Buratti, C., Belloni, E., Lunghi, L. & Barbanera, M. Thermal conductivity measurements by means of a new ‘Small Hot-Box’ apparatus: manufacturing, calibration and preliminary experimental tests on different materials. *Int. J. Thermophys.* **37**, 47 (2016).
58. Buratti, C., Moretti, E., Belloni, E. & Zinzi, M. Experimental and numerical energy assessment of a monolithic aerogel glazing unit for building applications. *Appl. Sci.* **9**, 5473 (2019).
59. Ohno, Y. *Color Rendering*, Proc. CIE 26th (CIE, 2007).
60. Glass in building—Determination of light transmittance, solar direct transmittance, total solar energy transmittance, ultraviolet transmittance and related glazing factors. ISO 9050:2003 (2003).
61. Born, M. & Wolf, E. *Principles of Optics* 7th edn (Cambridge Univ. Press, 1999).
62. Keating, M. P. *Geometric, Physical, and Visual Optics* 2nd edn (Butterworth-Heinemann, 2002).
63. Bellunato, T. et al. Refractive index of silica aerogel: Uniformity and dispersion law. *Nucl. Instrum. Methods Phys. Res. B* **595**, 183–186 (2008).
64. Charlet, E. & Grelet, E. Anisotropic light absorption, refractive indices, and orientational order parameter of unidirectionally aligned columnar liquid crystal films. *Phys. Rev. E* **78**, 041707 (2008).
65. McCluney, W. R. in *Encyclopedia of Energy Engineering and Technology* 2nd edn (ed. Anwar, S.) 2271–2281 (CRC Press, 2014).
66. Voluntary test method for thermal transmittance and condensation resistance of windows, door and glazed wall sections. AAMA 1503-09 (2009).
67. Mastronarde, D. N. Automated electron microscope tomography using robust prediction of specimen movements. *J. Struct. Biol.* **152**, 36–51 (2005).
68. Mastronarde, D. N. SerialEM: a program for tilt series acquisition on Tecnai microscopes using prediction of specimen position. *Microsc. Microanal.* **9**, 1182–1183 (2003).
69. *WINDOW 7 User Manual* (Lawrence Berkeley National Laboratory, 2019); <https://windows.lbl.gov/tools/window/documentation>

## Acknowledgements

We thank B. Borak, K. Burrows, T. Culp, J. Gerbi, B. Fleury, A. Hess, P. de Melo, E. Schiff, M. Sofos, R. Tenent and A. Repula for discussions. I.I.S. acknowledges hospitality of the International Institute for Sustainability with Knotted Chiral Meta Matter in Japan during part of his sabbatical stay, during which this paper was prepared for publication. We acknowledge support of the US Department of Energy, under the Advanced Research Projects Agency-Energy (ARPA-E) award DE-AR0000743.

## Author contributions

E.A., B.S., V.C., J.B.t.H., T.L., Q.L. and I.I.S. conducted experimental work and analysed data. T.L. and B.S. performed numerical modelling of the thermal barrier performance of SiCellA-based retrofits and IGUs. I.I.S. conceived and designed the project and wrote the paper, with contributions from all authors.

## Competing interests

The authors declare the following competing financial interests: I.I.S., Q.L., E.A., B.S., V.C. and T.L. filed patent applications related to cellulose aerogel technology submitted by the University of Colorado, and an additional patent is filed concurrently with this paper. The other authors declare no competing interests.

## Additional information

**Supplementary information** The online version contains supplementary material available at <https://doi.org/10.1038/s41560-023-01226-7>.

**Correspondence and requests for materials** should be addressed to Ivan I. Smalyukh.

**Peer review information** *Nature Energy* thanks Cinzia Buratti, Roel Loonen and the other, anonymous, reviewer(s) for their contribution to the peer review of this work.

**Reprints and permissions information** is available at [www.nature.com/reprints](http://www.nature.com/reprints).

**Publisher's note** Springer Nature remains neutral with regard to jurisdictional claims in published maps and institutional affiliations.

**Open Access** This article is licensed under a Creative Commons Attribution 4.0 International License, which permits use, sharing, adaptation, distribution and reproduction in any medium or format, as long as you give appropriate credit to the original author(s) and the source, provide a link to the Creative Commons license, and indicate

if changes were made. The images or other third party material in this article are included in the article's Creative Commons license, unless indicated otherwise in a credit line to the material. If material is not included in the article's Creative Commons license and your intended use is not permitted by statutory regulation or exceeds the permitted

use, you will need to obtain permission directly from the copyright holder. To view a copy of this license, visit <http://creativecommons.org/licenses/by/4.0/>.

© The Author(s) 2023